Dynamics of T cell activation mediated by eIF3 interactions with T cell receptor mRNAs

Dasmanthie De Silva[1,2], Lucas Ferguson[1], Benjamin E. Smith[3], Grant H. Chin[1], Ryan A. Apathy[4], Theodore L. Roth[4], Marek Kudla[1], Alexander Marson[4,5,6,7,8,9], Nicholas T. Ingolia[1,10], Jamie H. D. Cate[1,2,9,11,12]*

1. Department of Molecular and Cell Biology, University of California-Berkeley, Berkeley, California 94720, United States.
2. The J. David Gladstone Institutes, San Francisco, CA 94158 USA
3. School of Optometry, University of California, Berkeley, Berkeley, CA 94720, USA.
4. Department of Microbiology and Immunology, University of California, San Francisco, San Francisco, CA, USA.
5. Diabetes Center, University of California, San Francisco, San Francisco, CA, USA.
6. Chan Zuckerberg Biohub, San Francisco, CA, USA
7. Department of Medicine, University of California, San Francisco, San Francisco, CA, USA.
8. Parker Institute for Cancer Immunotherapy, San Francisco, CA, USA.
9. Innovative Genomics Institute, University of California, Berkeley, Berkeley, CA, USA.
10. California Institute for Quantitative Biosciences, University of California, Berkeley, Berkeley, United States.
11. Department of Chemistry, University of California-Berkeley, Berkeley, California 94720, United States.
12. Molecular Biophysics and Integrated Bioimaging Division, Lawrence Berkeley National Laboratory, Berkeley, California 94720, United States.

* Corresponding author: jcate@lbl.gov

Abstract

Activation of T cells requires a global surge in cellular protein synthesis, which is accompanied by a large increase in translation initiation[1–4]. A central component of the translation initiation machinery–the multi-subunit eukaryotic initiation factor 3 (eIF3)–is rapidly turned on when quiescent T cells are stimulated[3]. However, the precise role eIF3 plays in activated T cells is not known. Using a global transcriptome cross-linking approach, we show that human eIF3 interacts with a distinct set of mRNAs in activated Jurkat cells. A subset of these mRNAs, including those encoding the T cell receptor (TCR) subunits TCRA and TCRB, crosslink to eIF3 across the entire length of the mRNA. Fluorescence in situ hybridization studies reveal both *TCRA* and *TCRB* mRNAs form granules, potentially acting as translation "hot-spots." We further find that elements in the 3'-untranslated regions (3'-UTRs) of the *TCRA* and *TCRB* mRNAs that directly interact with eIF3 control the early dynamics of TCR translation and the extent of T cell activation. These results highlight a new role for eIF3 in regulation of translation dynamics and provide insights that can guide engineering of T cells for cell immunotherapy applications.

55 **Main**

56 Several lines of evidence indicate eIF3 serves specialized roles in cellular translation, by
57 recognizing specific RNA structures in the 5'-untranslated regions (5'-UTRs) of target
58 mRNAs[5], binding the 7-methyl-guanosine (m^7G) cap[6] or through interactions with *N*-6-
59 methyl-adenosine (m^6A) post-transcriptional modifications in mRNAs[7]. Binding to these
60 *cis*-regulatory elements in mRNA can lead to translation activation or repression,
61 depending on the RNA sequence and structural context[5,7,8]. These functions for eIF3 can
62 aid cell proliferation[5], or allow cells to rapidly adapt to stress such as heat shock[7].
63 Additionally, eIF3 plays an important role in the development of specific tissues[9–11].

64

65 In the immune system, T cell activation involves a burst in translation[1–4] and correlates
66 with assembly of subunit EIF3J with the main eIF3 complex[3]. However, whether eIF3
67 serves a general or more specific role in T cell activation is not known. To delineate how
68 eIF3 contributes to T cell activation, we first identified mRNAs that directly interact with
69 eIF3 in Jurkat cells activated for 5 hours with ionomycin and phorbol 12-myristate 13-
70 acetate (I+PMA), or in non-activated Jurkat cells as a control, using photoactivatable
71 ribonucleoside-enhanced crosslinking and immunoprecipitation (PAR-CLIP)[5,12,13] (**Fig.
72 1a**). We used Jurkat cells as a model for T cells, as PAR-CLIP experiments require a
73 large number of cells labeled with 4-thiouridine at a non-toxic concentration[14]. Jurkat cells
74 also have a defined T cell receptor and transcriptome, avoiding the donor-to-donor
75 variability of primary T cells. In the Jurkat PAR-CLIP experiments, RNA crosslinked to
76 eight of the thirteen eIF3 subunits, as identified by mass spectrometry: subunits EIF3A,
77 EIF3B, EIF3D and EIF3G as seen in HEK293T cells[5], as well as subunits EIF3C, EIF3E,

78 EIF3F, and EIF3L (**Fig. 1b, Extended Data Fig. 1, Supplementary Table 1**). In activated
79 Jurkat cells, eIF3 crosslinked to a substantially larger number of mRNAs compared to the
80 non-activated cells (**Extended Data Figs. 2 and 3, Supplementary Tables 2 and 3**).
81 Notably, eIF3 interacted with a completely new suite of mRNAs in activated Jurkat cells,
82 compared to those identified in HEK293T cells (**Fig 1c, Extended Data Fig. 4,**
83 **Supplementary Tables 4 and 5**). These mRNAs are enriched for those encoding
84 proteins central to immune cell function (**Supplementary Table 6**). Moreover, eIF3
85 crosslinking does not correlate with mRNA abundance (**Extended Data Fig. 4**),
86 suggesting that eIF3 is involved in specific regulation of T cell activation.
87
88 In activated Jurkat cells, eIF3 crosslinked to mRNAs by a multitude of patterns (**Fig 2a,**
89 **b, Extended Data Fig. 5**), consistent with varied roles for eIF3 in T cell activation and
90 function. Many of the mRNAs have a single PAR-CLIP site in the 5'-UTR as observed in
91 HEK293T cells[5] (**Fig. 2a**, **Extended Data Figs. 2, Supplementary Table 6**). However,
92 eIF3 crosslinked to some mRNAs across their entire length, from the beginning of the 5'-
93 UTR through the 3'-UTR (**Fig. 2a, b, Extended Data Fig. 5**). This "pan-mRNA" pattern of
94 eIF3 crosslinking–which includes polyadenylated mRNAs as well as histone mRNAs–has
95 not been observed before. Notably, a number of these mRNAs encode proteins important
96 for T cell activation, including both the alpha and beta subunits of the TCR, subunits TCRA
97 and TCRB (**Fig. 2b**, **Supplementary Table 6**).
98
99 Crosslinking in PAR-CLIP experiments requires direct interaction between the RNA and
100 protein of interest[14]. Thus, the pan-mRNA pattern of crosslinking between eIF3 and

101 certain mRNAs suggests formation of ribonucleoprotein complexes (RNPs) highly
102 enriched in eIF3. Remarkably, the pan-mRNA crosslinking pattern in the *TCRA* and *TCRB*
103 mRNAs occurs in activated but not non-activated Jurkat cells. As previously known RNPs
104 such as processing bodies (P bodies) and stress granules contain translationally
105 repressed mRNAs, we performed fluorescence in situ hybridization (FISH) on both *TCRA*
106 and *TCRB* mRNAs in activated Jurkat cells. Since Jurkat cells have a defined TCR, we
107 were able to design FISH probes across the entire *TCRA* and *TCRB* transcripts. We also
108 probed for P body and stress granule proteins DCP1 and G3BP1, respectively[15–18]. Both
109 the *TCRA* and *TCRB* mRNAs formed distinct puncta, but did not co-localize with either P
110 bodies or stress granules, or with each other (**Fig. 2c, Extended Data Fig. 6**). Taken
111 together, these results suggest that the *TCRA* and *TCRB* mRNA puncta represent eIF3-
112 mRNA concentrated regions that may act as translation "hot spots."
113
114 Both the *TCRA* and *TCRB* mRNAs include prominent sites of eIF3 crosslinking in their
115 respective 3'-UTR elements. To test the functional importance of these sites of eIF3
116 interaction, we used CRISPR-Cas9 genome editing with guide RNAs (gRNAs) targeted
117 to the two boundaries of the eIF3 PAR-CLIP sites in each of the 3'-UTRs of *TCRA* and
118 *TCRB* mRNA (**Extended Data Fig. 7, Supplementary Table 7**). We nucleofected these
119 pairs of gRNA/Cas9 RNPs into primary human T cells from two donors, to delete the
120 entire PAR-CLIP site in each 3'-UTR. PCR analysis showed successful deletion of the
121 eIF3 PAR-CLIP site in the *TCRA* 3'-UTR or in the *TCRB* 3'-UTR (*TCRA* Δ*PAR* or *TCRB*
122 Δ*PAR*, respectively) in approximately 50-60% of the cells (**Extended Data Fig. 7**). For
123 comparison with the *TCRA* Δ*PAR* or *TCRB* Δ*PAR* cell populations, we edited cells from

124 both donors using each gRNA targeting the *TCRA* 3'-UTR and *TCRB* 3'-UTR region
125 separately (single gRNA experiments), a gRNA targeting the coding sequence (CDS) of
126 *TCRA* which knocks out TCR expression with high efficiency (Δ*TCR*)[19], a scrambled
127 gRNA (SC) which does not cut anywhere in the human genome, and cells mixed with the
128 gRNA/Cas9 RNPs but not nucleofected.
129
130 We first measured total TCR protein levels in both the *TCRA* Δ*PAR* and *TCRB* Δ*PAR* cell
131 populations by western blot, after different times following T cell stimulation using anti-
132 CD3 and anti-CD28 antibodies (**Fig. 3a**). We used an anti-TCRA antibody to measure
133 TCR levels in both *TCRA* Δ*PAR* and *TCRB* Δ*PAR* cells, since the formation of an intact
134 TCR is required to stabilize both the TCRA and TCRB subunits[20,21]. In both *TCRA* Δ*PAR*
135 and *TCRB* Δ*PAR* cell populations, TCRA protein levels were nearly absent or clearly
136 reduced at early time points after activation (~1 hr). By contrast, SC control cells–which
137 should behave as wild-type T cells–exhibited a substantial burst in TCRA protein levels
138 immediately after activation (**Fig. 3a**). Only at later time points did TCRA levels in the
139 *TCRA* Δ*PAR* and *TCRB* Δ*PAR* cell populations begin to increase. Next we checked
140 whether the reduced TCR protein levels in *TCRA* Δ*PAR* and *TCRB* Δ*PAR* cell populations
141 at early time points after activation with anti-CD3 and anti-CD28 antibodies affected the
142 rate of TCR clustering, as occurs in immune synapse formation[22]. We used the same cell
143 populations as those for western blot analysis (**Fig. 3a**), to correlate the TCRA protein
144 levels observed in the western blots with TCR cluster formation. Using TCR protein
145 staining, we observed a decrease in the proportion of cells that formed TCR clusters in
146 the *TCRA* Δ*PAR* and *TCRB* Δ*PAR* cell populations compared to SC control cells, with

147 more severe defects seen at the earlier time points (**Fig. 3b**). We also stained cells with
148 a fluorescently tagged anti-TCR antibody and used flow cytometric analysis to measure
149 the levels of TCR on the cell surface with and without activation with I+PMA (**Fig. 3c, d,**
150 **Extended Data Fig. 8**). A substantially lower percentage of the *TCRA* Δ*PAR* and *TCRB*
151 Δ*PAR* cell populations expressed TCR on the cell surface compared to SC control cells
152 or cells edited with a single gRNA (**Fig. 3c, d, Extended Data Fig. 8**). Taken together,
153 these results suggest that regulation of TCR protein synthesis mediated by the *TCRA* and
154 *TCRB* mRNA 3'-UTR elements that interact with eIF3 is required for the robust TCR
155 clustering that is central to immune synapse formation[22].
156
157 To test whether the defect in TCR clustering in the *TCRA* Δ*PAR* and *TCRB* Δ*PAR* cell
158 populations reflects a general deficiency in T cell activation, we measured the T cell
159 activation markers CD69 and CD25 by flow cytometry and secreted cytokines IL2 and
160 IFNγ using ELISA (**Fig. 4, Extended Data Figs. 9–12**). Both the CD4+ and CD8+
161 Δ*TCR* cell populations failed to express significant amounts of CD69 and CD25 (**Fig.**
162 **4a,b, Extended Data Fig. 10, Extended Data Fig. 11**), and the Δ*TCR* cells only weakly
163 upregulated IL2 and IFNγ, particularly at the 24 hour time point (**Fig. 4c, Extended**
164 **Data Fig. 12**). Notably, fewer cells in the *TCRA* Δ*PAR* and *TCRB* Δ*PAR* CD4+ and
165 CD8+ cell populations expressed CD69 after 5 and 8 hours after activation, compared
166 to SC control CD4+ and CD8+ cells (**Fig. 4a,b, Extended Data Fig. 10, Extended Data**
167 **Fig. 11**). At later time points, fewer cells in the *TCRA* Δ*PAR* and *TCRB* Δ*PAR* cell
168 populations expressed both CD69 and CD25 activation markers compared to SC
169 control cells. Furthermore, the *TCRA* Δ*PAR* and *TCRB* Δ*PAR* T cell populations

170 secreted lower amounts of cytokines IL2 and IFNγ, compared to the SC control cells
171 (**Fig. 4c, Extended Data Fig. 12**). Taken together, the *TCRA* Δ*PAR* and *TCRB* Δ*PAR*
172 primary T cell populations exhibited activation defects at early and later time points, and
173 align with the decreased TCR levels observed by western blot, detected by TCR
174 clustering and by flow cytometry analyses (**Fig. 3**), consistent with eIF3-mediated
175 regulation of T cell activation through interactions with the *TCRA* and *TCRB* mRNA 3'-
176 UTR PAR-CLIP sites, in both CD4+ and CD8+ T cells.
177
178 To obtain a deeper mechanistic understanding of the role of eIF3 in the regulation of
179 TCRA and TCRB translation, we recreated the deletions of the eIF3 PAR-CLIP sites in
180 both the *TCRA* and *TCRB* mRNA 3'-UTRs (**Extended Data Fig. 7**) in Jurkat cells, which
181 can be clonally propagated for detailed analysis. As observed in edited primary T cells,
182 *TCRA* Δ*PAR* and *TCRB* Δ*PAR* Jurkat cell populations expressed lower levels of the TCR
183 proteins compared to wild-type (WT) cells, and failed to show a burst in TCR expression
184 at early time points after anti-CD3 and anti-CD28 activation (**Extended Data Fig. 13a**).
185 Notably, *TCRA* and *TCRB* mRNA levels were unaffected or even increased in the *TCRA*
186 Δ*PAR* and *TCRB* Δ*PAR* Jurkat cells (**Extended Data Fig. 13b, c**). Importantly, the
187 amount of *TCRA* and *TCRB* mRNAs interacting with eIF3 was higher in WT cells than in
188 the *TCRA* Δ*PAR* and *TCRB* Δ*PAR* cells after activation (**Extended Data Fig. 14**),
189 indicating that deleting the eIF3 PAR-CLIP sites disrupts eIF3 interactions with these
190 mRNAs. Additionally, the levels of eIF3-mRNA interaction closely mirrored the total *TCRA*
191 protein levels at both 5 hours and 8 hours for WT, *TCRA* Δ*PAR* and *TCRB* Δ*PAR* cells,
192 suggesting that eIF3 interactions with the 3'-UTR sequences in the *TCRA* and *TCRB*

193 mRNAs is tightly coupled with *TCRA* and *TCRB* protein levels. The *TCRA* Δ*PAR* and
194 *TCRB* Δ*PAR* Jurkat cells also showed a delay in TCR clustering (**Extended Data Fig.**
195 **15**), had lower cell populations expressing CD69 and CD25, and secreted lower amounts
196 of IL2 compared to WT cells (**Extended Data Fig. 16**), mirroring the results obtained in
197 primary T cells (**Fig. 4, Extended Data Fig. 10-12**). These results verify that Jurkat cells
198 recapitulate the response of primary T cells, and further support the model that eIF3
199 interactions with the PAR-CLIP sites in the *TCRA* and *TCRB* mRNA 3'-UTRs mediate
200 translational regulation at early times after TCR activation.
201
202 In order to understand the functional role of eIF3 interactions with the 3'-UTRs of the
203 *TCRA* and *TCRB* mRNAs, we constructed nanoluciferase reporters with the 5'-UTR of
204 the human beta globin gene (*HBB*) and a PEST destabilization domain. The PEST
205 domain reduces nanoluciferase protein half-life[23,24] and provides better time resolution of
206 nanoluciferase expression after T cell activation. The reporter coding sequence (CDS)
207 was then fused to the wild-type *TCRA* or *TCRB* mRNA 3'-UTR sequence (WT), or 3'-UTR
208 with the eIF3 PAR-CLIP site deleted (*ΔPAR*), or 3'-UTR with the reversed sequence of
209 the eIF3 PAR-CLIP site (R**PAR*, i.e. 5'-3' sequence reversed to 3'-5' direction) (**Fig. 5a**),
210 and stably transduced into Jurkat cells using a lentiviral vector. Cells expressing
211 nanoluciferase from reporters with a deletion or reversal of the eIF3 PAR-CLIP site
212 sequence led to reduction of the luminescence signal compared to cells expressing
213 nanoluciferase with the WT 3'-UTR sequences (**Fig. 5b**). Furthermore, similar to the
214 *TCRA* Δ*PAR* and *TCRB* Δ*PAR* Jurkat cell lines, there was no significant defect in the
215 *TCRA* Δ*PAR* and *TCRA* R**PAR* nanoluciferase mRNA levels compared to intact *TCRA*

216 3'-UTR mRNA, or for *TCRB* Δ*PAR* and R**PAR* nanoluciferase mRNA levels compared to
217 intact *TCRB* 3'-UTR mRNA through 5 hrs, when the biggest defect in luciferase translation
218 is observed (**Fig. 5c**). Immunoprecipitation of eIF3 followed by qRT-PCR quantification of
219 nanoluciferase mRNA showed that less nanoluciferase mRNA was bound to eIF3 when
220 the 3'-UTR PAR-CLIP site was either deleted or reversed, compared to nanoluciferase
221 mRNAs carrying the WT *TCRA* or *TCRB* 3'-UTR (**Fig. 5d**). These results support the
222 model that eIF3 binding to the PAR-CLIP sites in the *TCRA* and *TCRB* mRNA 3'-UTRs is
223 necessary for eIF3-mediated temporal regulation of TCRA and TCRB translation in
224 activated T cells.
225
226 Recent experiments indicate that T cells must cross a "threshold" of T cell receptor
227 signaling to commit to activation and proliferation[25,26], setting up a "digital" response to
228 antigen recognition[25–28]. The response threshold involves integration of intensity and
229 duration of TCR signaling[25,26,28], and spans a wide range of TCR antigen affinity[25–28].
230 Notably, T cell commitment to clonal expansion and differentiation can occur with as little
231 as 1 to 2 hours of TCR stimulation for effector CD4+ and naive CD8+ T cells[29,30]. This
232 time period spans the burst in TCR protein synthesis mediated by eIF3 interactions with
233 the *TCRA* and *TCRB* 3'-UTR elements (**Fig. 3a**). Naive CD4+ T cells require a longer
234 duration of TCR signaling of ~20 hours[29,31]. Although we were not able to distinguish
235 levels of TCR translation in isolated CD8+ and CD4+ cells (**Fig. 3**), subsequent events in
236 T cell activation including CD69 and CD25 expression, and IL2 and IFNγ secretion, were
237 equally affected in CD8+ and CD4+ cells in which the 3'-UTR PAR-CLIP sites were
238 deleted (**Fig. 3, Fig. 4**). Taken together, our results indicate eIF3 controls *TCRA* and

239 *TCRB* mRNA translation during the first critical hours after TCR stimulation that lead to
240 subsequent T cell commitment to proliferation and differentiation. These results also
241 suggest that eIF3-responsive mRNA 3'-UTR elements could be used to improve chimeric
242 antigen receptor (CAR) expression and CAR-T cell responsiveness[32,33].
243
244 The eIF3 PAR-CLIP experiment we present here provides a snapshot of eIF3-RNA
245 interactions that occur at the time TCR translation is most sensitive to eIF3 regulation (5
246 hours in Jurkat cells, **Fig. 2b**, **Extended Data Fig. 13**). At this point in time, eIF3
247 crosslinks to multiple mRNAs encoding proteins involved in immune cell function
248 (**Supplementary Table 6**). Interestingly, the patterns of eIF3 crosslinking, which for a
249 number of mRNAs include interactions with the protein coding sequence and 3'-UTR (**Fig.
250 2**, **Extended Data Fig. 5b**), suggest an active role for eIF3 in promoting translation of
251 these mRNAs. In support of this model, the two examples of pan-mRNAs we examined
252 here (*TCRA* and *TCRB*) reside in puncta distinct from P bodies and stress granules (**Fig.
253 2c**). However, this eIF3-mediated translation activation is transient, lasting only 1-2 hours
254 in primary T cells (**Fig. 3b**, **Extended Data Fig. 13a**). Recent evidence suggests that eIF3
255 can remain associated with translating ribosomes[34,35,36] a phenomenon that may be
256 enhanced for the pan-mRNAs identified here. Notably, additional layers of translation
257 regulation also contribute to T cell function[37], particularly with respect to mTOR
258 signaling[3,38] and carbon metabolism[4,39]. It should now be possible to use the present
259 PAR-CLIP experiments to elucidate additional roles for eIF3-mediated translation
260 regulation and to more fully map the system-wide role of translation regulation in T cell
261 activation.
262

263 **Figures**

264

265 **Figure 1. PAR-CLIP analysis of eIF3 interactions with RNAs in Jurkat cells. a**,
266 Schematic of Jurkat cell treatment with 4-thiouridine, activation, and cell harvesting for
267 PAR-CLIP analysis. **b**, Phosphorimage of SDS polyacrylamide gel resolving 5′ ^{32}P-
268 labeled RNAs crosslinked to eIF3 subunits in activated and non-activated Jurkat cells.
269 **c**, Venn diagram of genes identified by eIF3 PAR-CLIP in the two biological replicates of
270 activated Jurkat cells, compared with the eIF3 PAR-CLIP mRNAs identified in HEK293T
271 cells. The same number of mRNAs from the Jurkat cell PAR-CLIP libraries, ranked by
272 total reads mapped to a given gene, are compared to the number of mRNAs identified
273 in the HEK293T PAR-CLIP experiments.

274

275 **Figure 2. Varied mRNA crosslinking patterns to eIF3 in activated Jurkat cells. a**,
276 Cumulative plot showing mRNA crosslinking in sample EIF3A/C/B to predominantly the
277 5'-UTR (n = 396, 414 mRNAs in replicates 1 and 2, respectively), and across the entire
278 length of some mRNAs (n = 634, 621 mRNAs). We defined mRNAs having a ratio of
279 normalized 5'-UTR reads divided by 3'-UTR reads of 20 or more as "5'-UTR enriched"
280 with respect to eIF3 crosslinking. All others were categorized as "pan-mRNAs," with
281 eIF3 crosslinking across the entire length of the mRNA. The cut-off value 20 is not a
282 sharp boundary between the two categories of mRNA (**Extended Data Fig. 5a**). The 5'-
283 UTR, CDS, and 3'-UTR regions are shown normalized by length. **b**, Crosslinking of eIF3
284 subunits EIF3A/C/B, EIF3B/C and EIF3D/L across the entire *TCRA* and *TCRB* mRNAs.
285 5'-UTR, coding sequence (CDS), and 3'-UTR elements for the mapped TCR genes in

286 Jurkat cells are shown. Counts, PAR-CLIP reads from deep sequencing library
287 analysis[40]. **c**, FISH analysis of *TCRA* and *TCRB* mRNAs (yellow and magenta,
288 respectively) and P bodies (on the left) marked by the location of DCP1 (cyan) and
289 stress granules (on the right) marked by the location of G3BP1 (cyan), in activated
290 Jurkat cells. Graphs to the right of the images indicate Pearson's correlation coefficients
291 (PCCs) of *TCRA* and *TCRB* mRNA with each other or with P bodies or stress granules.
292 Labels on the x axis are, B: tetraSpeck microsphere beads, C: activated Jurkat cells. (n
293 = 5, P <0.008, for PCC values of cells relative to bead colocalization, across all the
294 channels tested, using the Wilcoxon rank-sum test). Images are representative of one
295 experiment of the five independent experiments in the graphs.
296
297 **Figure 3. TCR levels in activated primary human T cells with eIF3 3'-UTR PAR-**
298 **CLIP sites deleted. a**, Western blots measuring TCRA protein levels as a function of
299 time after anti-CD3/anti-CD28 activation. Cell lines used are labeled on the left: *TCRA*
300 Δ*PAR* (*TCRA* gRNA 1+2), *TCRB* Δ*PAR* (*TCRB* gRNA 1+2), and SC (scrambled gRNA).
301 HSP90 was used as a loading control. Schematics of *TCRA* and *TCRB* mRNAs with
302 and without eIF3 PAR-CLIP sites are shown above. SC control cells have the wild-type
303 (WT) 3'-UTRs for *TCRA* and *TCRB* mRNAs. **b**, The number of T cells with one or more
304 TCR clusters measured by anti-TCRA/anti-TCRB protein staining and epifluorescence
305 microscopy as a function of time after anti-CD3/anti-CD28 activation. A total of 100 cells
306 from each donor were imaged for *TCRA* Δ*PAR* (n = 2 donors, stained with anti-TCRA
307 antibody), *TCRB* Δ*PAR* (n = 2 donors, stained with anti-TCRB antibody), and SC cell
308 lines (n = 2 donors, each stained separately with anti-TCRA and anti-TCRB antibodies).

309 Values are mean ± standard deviation. P < 0.005 comparing *TCRA* Δ*PAR* and *TCRB*
310 Δ*PAR* to SC after 1 hour of activation. P ≤ 0.0002 comparing *TCRA* Δ*PAR* and *TCRB*
311 Δ*PAR* to SC after 3 hours of activation, using two-way ANOVA. **c**, Representative
312 density plots showing the percentage of I+PMA activated T cells expressing TCR on the
313 cell surface 3 hours after activation, measured by flow cytometric analysis for one of two
314 donors. The cell lines shown are *TCRA* Δ*PAR*, *TCRB* Δ*PAR*, Δ*TCR* (negative control),
315 and SC. **d**, Percent cells expressing TCR on the cell surface after I+PMA activation for 3
316 hours (*n* = *2* donors, with mean and standard deviation shown), reported in bar graph
317 form. P < 0.0001 for *TCRA* Δ*PAR* or *TCRB* Δ*PAR* relative to SC, using one-way
318 ANOVA.
319
320 **Figure 4. Phenotypic analysis of primary human T cells. a,** Flow cytometric analysis
321 measuring T cell activation markers CD69 (early activation marker) and CD25 (mid-
322 activation marker) in *TCRA* Δ*PAR*, *TCRB* Δ*PAR*, Δ*TCR* and SC CD8+ T cells,
323 quantifying mean percent cells expressing CD69+ only (left) and CD69+ CD25+ (right)
324 from (*n* = 2 donors). **b**, Density plots showing cell populations expressing CD69+ only,
325 CD69+ CD25+ or CD25+ only from one of the donors. Cells sorted as shown in
326 **Extended Data Fig. 9**. **c**, Quantification of secreted IL2 and IFNγ from cell lines *TCRA*
327 Δ*PAR, TCRB* Δ*PAR,* Δ*TCR* and SC cell populations from (*n* = 2 donors) at different
328 time points after stimulation with anti-CD3/anti-CD28 antibodies, as determined by
329 ELISA. For both figures **a,** and **c,** Values are mean ± standard deviation, ****P < 0.0001
330 relative to SC, using two-way ANOVA. Differences in expression of activation markers

331 and secreted cytokines in comparisons of *TCRA* Δ*PAR* with *TCRB* Δ*PAR* were not
332 significant.
333
334 **Figure 5. Role of the eIF3 PAR-CLIP sites in the 3'-UTRs of *TCRA* and *TCRB*,**
335 **measured by nanoluciferase reporters. a**, Schematic of the nanoluciferase reporters
336 stably expressed in Jurkat cells. WT, intact 3'-UTR from either *TCRA* or *TCRB* mRNA;
337 *ΔPAR*, 3'-UTR of *TCRA* or *TCRB* with the eIF3 PAR-CLIP site deleted (nucleotides 102-
338 338 in the 3'-UTR of *TCRA* mRNA or nucleotides 16-161 in the 3'-UTR of *TCRB*
339 mRNA); R**PAR*, reversed PAR-CLIP sequence in the 3'-UTR of *TCRA* or *TCRB* mRNA.
340 **b**, Luciferase activity in anti-CD3/anti-CD28 activated Jurkat cells, relative to non-
341 activated controls (n = 3, with mean and standard deviations shown). $P < 0.0001$ for
342 *TCRA* Δ*PAR* and R**PAR* relative to WT at 5 hr and 8 hr, and $P \leq 0.0002$ for 10 hr, using
343 two-way ANOVA. $P < 0.0001$ for *TCRB* Δ*PAR* and R**PAR* relative to WT for 1 hr - 10
344 hr. **c**, Changes in nanoluciferase mRNA levels in cells stably expressing the
345 nanoluciferase reporters activated with anti-CD3/anti-CD28 antibodies, as determined
346 by qRT-PCR. $P < 0.0001$ for *TCRA* Δ*PAR* relative to WT at 8 hr, and for *TCRA* Δ*PAR*
347 and R**PAR* relative to WT at 10 hr, using two-way ANOVA. $P \leq 0.0002$ for *TCRB* Δ*PAR*
348 and R**PAR* relative to WT at 8 hr and 10 hr. **d**, Immunoprecipitation of eIF3 using an
349 anti-EIF3B antibody[5], followed by qRT-PCR to quantify the amount of nanoluciferase
350 mRNA bound to eIF3 (n = 3, with mean and standard deviations shown). The schematic
351 of the experiment is indicated on the left. For *TCRA* and *TCRB* mRNAs, $P < 0.0001$ for
352 Δ*PAR* and R**PAR* relative to WT, using two-way ANOVA. P values for IL2 mRNAs for
353 Δ*PAR* and R**PAR* relative to WT were not significant.

354 **Materials and methods**

355 **Jurkat cell culture**

356 Human Jurkat, Clone E6-1 (ATCC TIB-152) was purchased from American Type
357 Culture Collection (ATCC) and was maintained in RPMI 1640 Medium (ATCC
358 modification) with 10% FBS (VWR Life Science Seradigm) and 0.01% Penicillin-
359 Streptomycin (10,000 U/mL). The cells were maintained between 1 million to 8 million
360 cells ml^{-1}. When cells were stimulated they were always maintained at 8 million
361 cells ml^{-1}.
362

363 **Isolation of human primary T cells**

364 Primary human T cells were isolated from healthy human donors from leukoreduction
365 chambers after Trima Apheresis (Vitalant, formerly Blood Centers of the Pacific).
366 Peripheral blood mononuclear cells (PBMCs) were isolated from whole blood samples
367 by Ficoll centrifugation using SepMate tubes (STEMCELL) per manufacturer's
368 instructions. T cells were isolated from PBMCs from all cell sources by magnetic
369 negative selection using an EasySep Human T Cell Isolation Kit (STEMCELL), per
370 manufacturer's instructions. Unless otherwise noted, isolated T cells were stimulated as
371 described below and used immediately.
372

373 **Primary human T cell culture**

374 Bulk T cells were cultured in XVivo15 medium (STEMCELL) with 5% fetal bovine serum
375 (FBS), 50 μM 2-mercaptoethanol, and 10 μM *N*-acetyl-cystine. Immediately after
376 isolation, T cells were stimulated for 2 days with anti-human CD3/CD28 magnetic

377 Dynabeads (ThermoFisher) at a bead to cell concentration of 1:1, along with cytokine
378 IL-2 at 500 U ml^{-1} (UCSF Pharmacy). After electroporation, T cells were cultured in
379 media with IL-2 at 500 U ml^{-1}. Throughout the culture period T cells were maintained at
380 an approximate density of 1 million cells per mL of media. Every 2–3 days after
381 electroporation, additional media was added, along with additional fresh IL-2 to bring the
382 final concentration to 500 U/mL, and the cells were transferred to larger culture flasks as
383 necessary to maintain a density of 1 million cells ml^{-1}.
384
385 For the T cell stimulation assay, edited primary T cells were transferred to fresh media
386 lacking IL2 after 9 days of culturing. The T cells were then stimulated with anti-CD3 and
387 anti-CD28 antibodies using flat bottom plates coated with anti-CD3 antibody (at a 10 µg
388 ml^{-1} concentration), and anti-CD28 antibody added to the cell culture media at a
389 concentration of 5 µg ml^{-1}.
390
391 **Jurkat cell stimulation**
392 The Jurkat cells used for the for the PAR-CLIP experiment were stimulated with 1X Cell
393 Stimulation Cocktail, containing phorbol 12-myristate 13-acetate (PMA) and ionomycin
394 (Thermofisher, Catalog number: 00-4970-93). Unless otherwise stated all other Jurkat
395 cell simulations were performed with anti-CD3 and anti-CD28 antibodies (Tonbo). Flat
396 bottom plates were coated with anti-CD3 antibody (at a 10 µg ml^{-1} concentration), and
397 anti-CD28 antibody was added to the cell culture media at a concentration of 5 µg ml^{-1}.
398
399 **4-thiouridine optimization**

400 Jurkat cells were seeded, so that they reached $8X10^5$ cells ml^{-1} seeding density on the
401 day of the experiment. Varying concentrations of s4U were added to the cells (50 μM,
402 75 μM, 100 μM, or none as a negative control). The cells were then incubated for
403 different time points: 8 hours, 10 hours, 12 hours, or 16 hours. After each incubation
404 time cell viability was determined using the CellTiter-Glo assay (Promega), according to
405 the manufacturer's instructions. Concentrations at which the relative luminescence in
406 the presence of s4U (luminescence of the s4U treated cells/luminescence of the
407 untreated cells) exceeded 95% were considered non-toxic. Based on these
408 measurements, we used 50 μM of 4-thiouridine for PAR-CLIP experiments.
409

410 **PAR-CLIP**

411 Two biological replicates were used to perform PAR-CLIP analysis as described in[5],
412 with modifications for Jurkat cells. 50 μM of 4-thiouridine was determined as non-toxic to
413 Jurkat cells over the time course of the PAR-CLIP experiments[14]. A total of 55 million
414 Jurkat cells seeded at 8 million cells ml^{-1} was treated with 50 μM of 4-thiouridine
415 (Sigma) for 7 hours, then stimulated with 1X Cell Stimulation Cocktail for 5 hours in
416 media containing 50 μM of 4-thiouridine (**Fig. 1a**). The same number of cells were
417 treated with 50 μM of 4-thiouridine (Sigma) for 12 hours without stimulation as a non-
418 activated control. The cells were then crosslinked on ice with 365 nm UV irradiation at
419 an energy dose of 0.2 J cm^{-2}. The cells were pelleted by centrifugation at 100 x g for 15
420 min at 4 °C, and the pellet was resuspended in three volumes of NP40 lysis buffer (50
421 mM HEPES-KOH pH 7.5, 150 mM KCl, 2 mM EDTA, 0.5% Nonidet P-40 alternative, 0.5
422 mM dithiothreitol (DTT), 1 Complete Mini EDTA-free Protease Inhibitor Cocktail tablet

423 (Roche)). The cell suspension was then incubated on ice for 10 min, passed through an
424 18G needle five times, and centrifuged at 13,000 x g for 15 min at 4 °C and RNAs were
425 lightly digested by treatment with MNase (Thermo Scientific) at a final concentration of
426 0.05 U μl^{-1} for 20 min at 16 °C. For each PAR-CLIP assay 1000 µl of Dynabeads
427 (Invitrogen) and 800 µl of anti-EIF3B antibody (Bethyl A301-761A) were used. The
428 remaining steps of the PAR-CLIP analysis was performed exactly as described in [5,41]
429 with the exception of using MNase at 5 U μl^{-1} for the on-bead digestion step.
430

431 **PAR-CLIP computational analysis**

432 PAR-CLIP cDNA libraries were sequenced on an Illumina HiSeq 2500 platform. To
433 eliminate potential PCR biases during PAR-CLIP library preparation, a random bar code
434 was introduced into the 3' adapter and all the reads that matched the random barcode
435 were collapsed into single reads. Clusters of overlapping sequence reads mapped
436 against the human genome version hg38 were generated using the PARalyzer software
437 [40] incorporated into the PARpipe pipeline (https://ohlerlab.mdc-
438 berlin.de/software/PARpipe_119/, [13]) with the settings below. Binding sites were
439 categorized using the Gencode GRCh38.p12 GTF annotations
440 (gencode.v21.annotation.gtf), https://www.gencodegenes.org/human/.
441

442 The PARpipe settings used were:
443 Conversion = T>C
444 Minimum read count per group = 5
445 Minimum read count per cluster = 7

446 Minimum read count for kde = 3

447 Minimum cluster size = 11

448 Minimum conversion locations for cluster = 2

449 Minimum conversion count for cluster = 2

450 Minimum read count for cluster inclusion = 1

451 Minimum read length = 20

452 Maximum number of non conversion mismatches = 1

453

454 **Comparison of eIF3 PAR-CLIP results in Jurkat and HEK293T cells**

455 To compare RNAs in activated Jurkat cells crosslinked to eIF3 with those crosslinked to
456 eIF3 in HEK293T cells[5], the gene cluster lists (*.gene_cl.csv) from APA_REP1,
457 APA_REP2, APB_REP1, APB_REP2, APD_REP1, and APD_REP2 were used (see
458 **Supplementary Table 3**). The genes were first sorted by total read counts
459 ("ReadCountSum") from high to low for each library to obtain the top candidate genes.
460 Then, the same number of top candidate genes from these sorted lists as the number of
461 genes identified in HEK293T cells, for eIF3 subunit EIF3A, EIF3B, and EIF3D
462 crosslinked to RNA[5], were chosen for comparison.

463

464 **PAR-CLIP Pathway analysis**

465 To determine biological pathways enriched in the set of mRNAs that crosslinked to eIF3
466 in activated Jurkat cells, genes with at least 100 total aligned reads were used, as
467 determined in the PARpipe analysis described above[13], from the EIF3A/C/B samples.
468 Since PAR-CLIP reads are short, it is not possible to determine with certainty which

469 mRNA transcript isoform cross-linked with eIF3. Therefore the most abundant mRNA
470 transcript isoform for each gene was chosen, as determined by transcriptome profiling
471 using kallisto (protein_coding category)[42], as described in the Transcriptome Profiling
472 section. Even with this choice, eIF3 crosslinks to mRNAs do not correlate with mRNA
473 abundance (**Extended Data Figure 4b**). Human genome GRCh38.p13 annotation was
474 used to extract mRNA lengths by 5'-UTR, coding region and 3'-UTR (Ensembl
475 Biomart)[43]. These genes were then sorted by the density of PAR-CLIP reads in the
476 mRNA 5'-UTR region, prior to mapping pathways of transcripts that cross-linked to eIF3.
477 Due to the complexity of *TCRA* and *TCRB* transcript annotation, these transcripts were
478 excluded from the normalization calculation, but included in the pathway analysis. The
479 top 500 genes from the resulting EIF3A/C/B PAR-CLIP gene lists were used, sorted as
480 described above, to analyze gene enrichment profiles in the STRING database[44]. The
481 top tissue-specific categories involve the immune system and T cell function
482 (**Supplementary Table 6**). Note that the STRING database does not include TCR
483 subunits in its analysis.
484
485 **Metagene analysis**
486 The PAR-CLIP genes sorted as described above in the "PAR-CLIP pathway analysis"
487 were used and mapped against the most abundant mRNA transcript isoforms to
488 generate cumulative plots of the reads. Reads for the *TCRA* and *TCRB* mRNAs were
489 manually extracted from the Bowtie version 1.0.0 Hg38 alignment of the eIF3 PAR-CLIP
490 reads. These reads were combined with the mapped reads in the *.read.csv files
491 generated by Parpipe. The combined reads were then sorted to extract only reads

492 annotated as 5'-UTR, start codon, coding, stop codon, and 3'-UTR. The most abundant
493 transcript isoform, as identified in the transcriptome profiling using kallisto (described
494 below) was used. Reads mapped to the 5'-UTR and start codon were normalized by the
495 length of the 5'-UTR. Reads mapped to the coding region and stop codon were
496 normalized by the length of the coding region. Finally, reads mapped to the 3'-UTR
497 were normalized to the length of the 3'-UTR. Relative positions of the mapped reads
498 along a metagene were computed based on the locations each mapped read fell within
499 its respective feature. Relative positions were from -1 to 0 for the 5'-UTR, 0 to 1 for the
500 coding region, and 1 to 2 for the 3'-UTR. 5'-UTR values were computed by multiplying
501 the relative position by -1, whereas the 3-UTR values were were computed by adding 1
502 to the relative position. Coding region relative positions were unchanged. The empirical
503 cumulative distribution frequency function from R package ggplot2[45] was used to build
504 the metagene plots from the vector of relative positions for the reads which mapped to a
505 given set of reads.
506
507 We defined mRNAs having a ratio of normalized 5'-UTR reads divided by 3'-UTR reads
508 of 20 or more as 5'-UTR enriched with respect to eIF3 crosslinking. All others were
509 categorized as mRNAs with eIF3 crosslinking across the entire length of the mRNA.
510 The cut-off value 20 is not a sharp boundary between the two categories of mRNA
511 (**Extended Data Fig. 5a**).
512
513 **Transcriptome Profiling**

514 RNA samples were extracted from HEK293T cells, non-activated Jurkat cells, and
515 Jurkat cells activated for 5 hr with I+PMA, using the Direct-zol RNA Miniprep kit
516 (Zymoresearch). The libraries were prepared using TruSeq Stranded RNA LT Ribo-Zero
517 Gold kit (Illumina) following the manufacturer's instructions, with two biological
518 replicates per condition. Cutadapt (version 2.6)[46] with a minimum read length of 20, 5'
519 end with a cutoff of 15 and the 3' end with a cutoff of 10 in paired-end mode was used
520 to remove adapters. RNA-seq reads were pseudoaligned using kallisto v.0.46.0 run in
521 quant mode with default parameters to estimate transcript abundance (transcripts per
522 million, TPM)[42]. The transcript index for kallisto was made with default parameters and
523 GENCODE Release 32 (GRCh38.p13) FASTA file[47].
524
525 To compare HEK293T or non-activated Jurkat mRNA abundance with that in activated
526 Jurkat cells, the output from kallisto was used for analysis using DeSeq2 (ref [48]). All
527 protein-coding transcripts (protein_coding) were then selected for the comparisons,
528 using tximport[49] as part of the Bioconductor environment in R. All genes with ≥ 50 reads
529 summed across all four samples in a comparison (two biological replicates per
530 condition) were then used. Prior to making MA plots, the Approximate Posterior
531 Estimation for generalized linear model (apeglm) shrinkage estimator for log fold
532 changes was used[50] DeSeq2 output in **Supplementary Table 5** is presented prior to
533 shrinkage analysis.
534
535 **Mass spectrometry**

536 To identify eIF3 subunits that crosslinked with RNAs in the PAR-CLIP experiments, a
537 portion of eIF3 immunoprecipitated using Dynabeads as described above were treated
538 with nonradioactive ATP during the T4 PNK labeling step. The nonradioactive samples
539 were then run on the same gel next to the radiolabeled PAR-CLIP samples, Coomassie
540 stained (Pierce) and the bands that matched with the phosphorimager printout were
541 excised from the gel and submitted for identification using one-dimensional LC-MS/MS
542 (**Supplementary Table 1**).
543
544 **sgRNA/Cas9 RNP production**
545 The sgRNA/Cas9 RNPs used to edit Jurkat cells were produced by complexing sgRNA
546 (Synthego) to Cas9 as described[51] while RNPs to edit Primary Human T cells were
547 produced by complexing a two-component gRNA (crRNA and tracrRNA, Dharmacon) to
548 Cas9 as described in[19]. The targeting sequences for the sgRNAs and crRNA are given
549 in **Supplementary Table 7**. Recombinant Cas9-NLS was obtained from MacroLab in
550 the California Institute for Quantitative Biosciences.
551
552 **Jurkat and primary T cell genome editing**
553 Jurkat cells used for electroporation were collected at passage 5 or lower and were
554 maintained at a seeding density of 8 million cells ml^{-1} or lower. Primary T cells were
555 isolated as described above. Prior to electroporation the Primary T cells were stimulated
556 with magnetic anti-CD3/anti-CD28 Dynabeads (ThermoFisher) for 48 hours. After 48
557 hours these beads were removed from the cells by placing cells on an EasySep cell
558 separation magnet for 2 min before electroporation. One million Jurkat (not activated)

559 or primary T cells cells (activated with anti-CD3/anti-CD28 Dynabeads for 48 hours)
560 were rinsed with PBS and then resuspended in 20 µl of Lonza electroporation buffer P3.
561 The cells were then mixed with 2.5 µl Cas9 RNPs (50 pmol total) along with 2 µl of a
562 127-nucleotide non-specific single-stranded DNA oligonucleotide at 2 µg $µl^{-1}$ (4 µg
563 ssDNA oligonucleotide total). The cells were then electroporated per well using a Lonza
564 4D 96-well electroporation system with pulse code DN100 for Jurkat cells and EH115
565 for primary human T cells. Immediately after electroporation, 80 µl of pre-warmed
566 media (without cytokines) was added to each well, and the cells were allowed to rest for
567 15 min at 37 °C in a cell culture incubator while remaining in electroporation cuvettes.
568 After 15 min, cells were moved to final culture flasks.
569

570 **Western Blot**

571 Western blot analysis was performed using the following antibodies: anti-TCRA (SC-
572 515719), anti-HSP90 (SC-69703) (**Supplementary Table 7**).
573

574 **Total mRNA isolation and quantitative RT-PCR analysis**

575 Total RNA was isolated from whole cells for qRT-PCR using Quick RNA miniprep plus
576 kit from Zymo Research following the manufacturer's instructions. Quantitative RT-PCR
577 analysis was performed using the Power SYBR Green RNA-to-Ct 1-Step kit (Applied
578 Biosystems) according to the manufacturer's instructions, and the QuantStudio™ 3
579 Real-Time PCR System (ThermoFisher). Each target mRNA was quantified in three
580 biological replicates, with each biological replicate having three technical replicates.
581

582 **Plasmids**

583 The *TCRA* 3'-UTR and *TCRB* 3'-UTR sequences were amplified from Jurkat genomic
584 DNA. The nanoluciferease sequence fused to a PEST domain was amplified from
585 pNL1.2[*NlucP*] Vector Sequence (Promega) and was cloned into a modified CD813A
586 vector (System Biosciences) containing the beta-globin (*HBB*) 5'-UTR using the In-
587 Fusion® HD Cloning Kit (Takara). The subsequent mutations in the *TCRA* and *TCRB*
588 3'-UTRs were generated using these initial constructs. Both *TCRA/TCRB* Δ*PAR or*
589 *R*PAR* sequences were purchased as gblocks from IDT and were cloned into this
590 plasmid backbone.

591

592 **Generation of stable Jurkat cell lines expressing nanoluciferase reporter**

593 For lentiviral production HEK293T cells were plated at a density of 80% in T-75 flasks
594 the night before transfection. The cells were then transfected with plasmids: expressing
595 the nanoluciferase, PsPAX2 and pCMV-VSV-G using the Lipofectamine 3000 reagent
596 (ThermoFisher) following the manufacturer's instructions. Forty-eight hours after
597 transfection, the viral supernatant was collected, filtered and concentrated using PEG-it
598 Virus Precipitation Solution (System Biosciences) following the manufacturer's
599 instructions. The virus pellets were then resuspended in RPMI-1640 media and stored
600 in -80°C.

601

602 The Jurkat cell transductions were done with multiple viral titers using TransDux™ MAX
603 Lentivirus Transduction Reagent (System Biosciences) following the manufacturer's
604 instructions. To test the viral transduction efficiency of the cells, forty-eight hours after

605 viral transduction the percent of cells expressing GFP was measured by FACS analysis
606 and cells expressing less than 15% GFP was treated with 1μg ml^{-1} puromycin to the
607 media. The cells were maintained in media with 1μg ml^{-1} puromycin, but transferred into
608 media without puromycin the day before the cells were used for assays.
609

610 **Luciferase reporter assay**

611 The stable cell lines expressing the Nanoluciferease reporter were stimulated with anti-
612 CD3 and anti-CD28 antibodies and the nanoluciferase activity was assayed after 1 hr, 3
613 hr, 5 hr, 8 hr, 10 hr and 24 hrs after stimulation using Nano-Glo® Luciferase Assay
614 System (Promega). For each time point 200,000 cells were tested in triplicate for each
615 cell line.
616

617 **RNA immunoprecipitation and qPCR**

618 The EIF3B-RNA immunoprecipitations were carried out following the exact same
619 conditions used for the PAR-CLIP analysis with the following changes. For each
620 immunoprecipitation, cell lysates were prepared in NP40 lysis buffer (50 mM HEPES-
621 KOH pH 7.5, 150 mM KCl, 2 mM EDTA, 0.5% Nonidet P-40 alternative, 0.5 mM DTT, 1
622 Complete EDTA-free Proteinase Inhibitor Cocktail tablet per 50 ml of buffer) with 4
623 million cells. The lysates were then incubated with 50 μl Protein G Dynabeads
624 conjugated with 20 μl of anti-EIF3B antibody (Bethyl A301-761A) for two hours at 4 °C.
625 After incubation, the flow through was removed and the beads were washed three times
626 with 1 ml NP40 lysis buffer for each wash. The beads were then resuspended in 400 μl
627 TRIzol reagent (ThermoFisher) and vortexed for 1 minute. The RNA was extracted

628 following the manufacturer's instructions and qPCR was performed as described above
629 using primers listed in **Supplementary Table 7**.
630
631 **Flow cytometry and cell sorting**
632 Flow cytometric analysis was performed on an Attune NxT Acoustic Focusing
633 Cytometer (ThermoFisher). Surface staining for flow cytometry and cell sorting was
634 performed by pelleting cells and resuspending in 50 µl of FACS buffer (2% FBS in PBS)
635 with antibodies at the indicated concentrations (**Supplementary Table 7**) for 20 min at
636 4 °C in the dark. Cells were washed twice in FACS buffer before resuspension.
637
638 **ELISA**
639 The cell suspensions were collected after each time point of activation with anti-
640 CD3/anti-CD28 antibodies for WT, *TCRA* Δ*PAR* or *TCRB* Δ*PAR* cells. For each
641 timepoint the same number of cells were used from each strain to be able to compare
642 across strains and time points. The amount of secreted IL2 in the cell suspensions after
643 activation anti-CD3/anti-CD28 antibodies for WT, *TCRA* Δ*PAR* or *TCRB* Δ*PAR* cells
644 were measured by ELISA MAX™ Deluxe Set Human IL-2 (BioLegend) according to the
645 manufacturer's instructions.
646
647 **RNA-FISH and immunofluorescence**
648 Jurkat cells were washed with PBS, fixed with 3.7% (vol./vol.) formaldehyde for 10 min
649 at room temperature and washed three times with PBS. PBS was discarded and 1 ml
650 70% ethanol was added. The cells were incubated at 4 °C for 16 hours. The 70%

651 ethanol was aspirated and the cells were washed once with 0.5 ml Stellaris RNA wash
652 buffer A (Biosearch technologies). The cells were then incubated with 100 µl Stellaris
653 hybridization buffer (Biosearch Technologies) containing Stellaris RNA FISH probes
654 (Biosearch Technologies) at a final concentration of 125 nM (**Supplementary Table 7)**
655 and with the relevant antibody (**Supplementary Table 7)** for 16 hours at 28 °C. The
656 cells were then washed twice with 0.5 ml Stellaris RNA wash buffer A containing
657 secondary antibody conjugated with a fluorophore for 30 minutes at 37 °C in the dark.
658 The second Stellaris RNA wash buffer A contained DAPI in addition to the secondary
659 antibody. Finally the cells were washed once with 0.5 mL Stellaris RNA wash buffer B
660 and mounted with mounting solution (Invitrogen). All high resolution images were taken
661 using confocal ZEISS LSM 880 in Airyscan super-resolution mode, equipped withA
662 Plan-Apochromat 63x/1.4 Oil objective (Zeiss). To measure colocalization of *TCRA* and
663 *TCRB* mRNAs with each other or with P bodies (using DCP1 antibody) or stress
664 granules (G3BP1 antibody) the cells were mounted along with 0.1 µm TetraSpeck™
665 microspheres (ThermoFisher) adhered to the slide according to manufacturer's
666 instructions, to be able to account for the chromatic shift during image acquisition. For
667 the counting of cells containing TCR clusters, a Revolve Epi-Fluorescence microscope
668 (Echo), equipped with an A Plan-Apochromat 40x objective (Olympus) was used.
669

670 **Colocalization analysis**

671 To measure colocalization of *TCRA* and *TCRB* mRNAs with each other or with P bodies
672 (using DCP1 antibody) or stress granules (G3BP1 antibody), immunofluorescently
673 labelled cells (see above) were mounted along with 0.1 µm TetraSpeck™ microspheres

674 (ThermoFisher) adhered to the slide according to manufacturer's instructions, to be able
675 to account for the lateral and axial chromatic aberrations during image acquisition.
676
677 Z-stacks were acquired with 35 nm x 35 nm x 190 nm voxels on a ZEISS LSM 880 in
678 Airyscan super-resolution mode, equipped with a Plan-Apochromat 63x/1.4 Oil objective
679 (Zeiss). The images were then deconvolved to a lateral resolution of ≈150 nm and an
680 axial resolution of ≈500 nm (as confirmed by observing the discrete Fourier transform of
681 the z-stacks). After imaging a single cell, beads that were on the slide axial to the cell
682 were imaged to measure the corresponding lateral and axial chromatic aberrations.
683
684 To quantify the relative colocalization, we developed an automated processing and
685 analysis pipeline in ImageJ 1.52p available on github:
686 https://github.com/Llamero/TCR_colocalization_analysis-macro. Specifically, the
687 chromatic aberrations in the z-stacks were compensated for by registering the channels
688 of the bead z-stack to one another, and then applying the same registration vectors to
689 the corresponding channels in the cell z-stack[52]. Each channel of a z-stack was then
690 thresholded to remove background in the image, and then the colocalization between
691 each pair of images was measured using the Pearson's correlation coefficient.
692 Samples in which any pair of channels in the bead z-stack had a correlation of less than
693 0.45 were removed from final analysis, as this suggested that the images had
694 insufficient dynamic range in at least one of the channels for an accurate deconvolution.
695
696 **Data and Code Availability**

697 Sequencing data supporting the findings in this study have been deposited in the Gene
698 Expression Omnibus (GEO) Database (https://www.ncbi.nlm.nih.gov/geo/), with
699 accession codes _____. Code used to analyze the microscopy images is available on
700 github at https://github.com/Llamero/TCR_colocalization_analysis-macro. Raw data for
701 **Figure 3a**, **Extended Data Figure 1b**, and **Extended Data Figure 13a** are provided in
702 Supplementary Figures 1-3.
703

704 **Acknowledgements**

705 We thank M. Hafner for advice on PAR-CLIP methodology and data analysis, H. Nolla
706 and A. Valeros at the UC Berkeley flow cytometry facility for helping out with the FACS
707 analysis and single cell sorting, F. Ives and H. L. Aaron at the UC Berkeley Imaging
708 center for help with microscopy, J. Lui for advice on planning experiments and for
709 suggestions on the manuscript, and M. Mignardi for advice on FISH experiments. This
710 work was supported by NIH grant R01-GM065050 (J.H.D.C.) and a grant from the Tang
711 Prize for Biopharmaceutical Science (J.H.D.C.). N.T.I. is a Damon Runyon-Rachleff
712 Innovator (DRR#37-15) and NIH New Innovator (DP2 CA195768). A.M. holds a Career
713 Award for Medical Scientists from the Burroughs Wellcome Fund, is an investigator at
714 the Chan Zuckerberg Biohub and has received funding from the Innovative Genomics
715 Institute (IGI) and the Parker Institute for Cancer Immunotherapy (PICI). B.E.S. is
716 supported by NIH grant P30EY003176. Imaging experiments were conducted at the
717 Cancer Research Laboratory Molecular Imaging Center, supported by Helen Wills
718 Neuroscience Institute. Sequencing was carried out at the UCSF Center for Advanced

719 Technology and at the Vincent J. Coates Genomics Sequencing Laboratory at UC
720 Berkeley, supported by NIH grant S10 OD018174.

721

722 **Author Contributions**

723 Project and experiments were conceived and designed by D.D.S. and J.H.D.C. D.D.S.
724 carried out all experiments, with assistance from B.E.S. and G.H.C. for image
725 acquisition and analysis, from T.R., R.A.A., and A.M. for primary T cell genome editing
726 and cell culture protocols, and from L.F., M.K., N.T.I. and J.H.D.C. for analysis of the
727 deep sequencing-based experiments. The manuscript was written by D.D.S. and
728 J.H.D.C., with editing by all authors.

729

730 **Competing Interests**

731 The authors declare competing financial interests: T.L.R. and A.M. are co-founders of
732 Arsenal Therapeutics. A.M. is a co-founder of Spotlight Therapeutics. A.M. serves on the
733 scientific advisory board of PACT Pharma, is an advisor to Trizell and was a former
734 advisor to Juno Therapeutics. The Marson Laboratory has received sponsored research
735 support from Juno Therapeutics, Epinomics, Sanofi and a gift from Gilead. A provisional
736 patent application has been filed on some of the work presented herein.

737

738 **Materials and Correspondence**

739 Correspondence and requests for materials should be addressed to J.H.D.C.,
740 jcate@lbl.gov.

741

742

743 **Bibliography**

744 1. Ahern, T., Sampson, J. & Kay, J. E. Initiation of protein synthesis during
745 lymphocyte stimulation. *Nature* **248**, 519–521 (1974).
746 2. Kleijn, M. & Proud, C. G. The regulation of protein synthesis and translation factors
747 by CD3 and CD28 in human primary T lymphocytes. *BMC Biochem.* **3**, 11 (2002).
748 3. Miyamoto, S., Patel, P. & Hershey, J. W. B. Changes in ribosomal binding activity
749 of eIF3 correlate with increased translation rates during activation of T
750 lymphocytes. *J. Biol. Chem.* **280**, 28251–28264 (2005).
751 4. Ricciardi, S. *et al.* The Translational Machinery of Human CD4+ T Cells Is Poised
752 for Activation and Controls the Switch from Quiescence to Metabolic Remodeling.
753 *Cell Metab.* **28**, 895–906.e5 (2018).
754 5. Lee, A. S. Y., Kranzusch, P. J. & Cate, J. H. D. eIF3 targets cell-proliferation
755 messenger RNAs for translational activation or repression. *Nature* **522**, 111–114
756 (2015).
757 6. Lee, A. S., Kranzusch, P. J., Doudna, J. A. & Cate, J. H. D. eIF3d is an mRNA cap-
758 binding protein that is required for specialized translation initiation. *Nature* **536**, 96–
759 99 (2016).
760 7. Meyer, K. D. *et al.* 5' UTR m(6)A Promotes Cap-Independent Translation. *Cell* **163**,
761 999–1010 (2015).
762 8. de la Parra, C. *et al.* A widespread alternate form of cap-dependent mRNA
763 translation initiation. *Nat. Commun.* **9**, 3068 (2018).
764 9. Curran, S. P. & Ruvkun, G. Lifespan regulation by evolutionarily conserved genes
765 essential for viability. *PLoS Genet.* **3**, e56 (2007).

766 10. Choudhuri, A., Maitra, U. & Evans, T. Translation initiation factor eIF3h targets
767 specific transcripts to polysomes during embryogenesis. *Proc. Natl. Acad. Sci. U.*
768 *S. A.* **110**, 9818–9823 (2013).
769 11. Cattie, D. J. *et al.* Mutations in Nonessential eIF3k and eIF3l Genes Confer
770 Lifespan Extension and Enhanced Resistance to ER Stress in Caenorhabditis
771 elegans. *PLoS Genet.* **12**, e1006326 (2016).
772 12. Hafner, M. *et al.* Transcriptome-wide identification of RNA-binding protein and
773 microRNA target sites by PAR-CLIP. *Cell* **141**, 129–141 (2010).
774 13. Mukherjee, N. *et al.* Deciphering human ribonucleoprotein regulatory networks.
775 *Nucleic Acids Res.* **47**, 570–581 (2019).
776 14. Ascano, M., Hafner, M., Cekan, P., Gerstberger, S. & Tuschl, T. Identification of
777 RNA-protein interaction networks using PAR-CLIP. *Wiley Interdiscip. Rev. RNA* **3**,
778 159–177 (2012).
779 15. Hubstenberger, A. *et al.* P-Body Purification Reveals the Condensation of
780 Repressed mRNA Regulons. *Mol. Cell* **68**, 144–157.e5 (2017).
781 16. Aizer, A. *et al.* Quantifying mRNA targeting to P-bodies in living human cells
782 reveals their dual role in mRNA decay and storage. *J. Cell Sci.* **127**, 4443–4456
783 (2014).
784 17. Aulas, A. *et al.* G3BP1 promotes stress-induced RNA granule interactions to
785 preserve polyadenylated mRNA. *J. Cell Biol.* **209**, 73–84 (2015).
786 18. Protter, D. S. W. & Parker, R. Principles and Properties of Stress Granules. *Trends*
787 *Cell Biol.* **26**, 668–679 (2016).
788 19. Roth, T. L. *et al.* Reprogramming human T cell function and specificity with non-

789 viral genome targeting. *Nature* **559**, 405–409 (2018).

790 20. Ohashi, P. S. *et al.* Reconstitution of an active surface T3/T-cell antigen receptor by
791 DNA transfer. *Nature* **316**, 606–609 (1985).

792 21. Koning, F., Lew, A. M., Maloy, W. L., Valas, R. & Coligan, J. E. The biosynthesis
793 and assembly of T cell receptor alpha- and beta-chains with the CD3 complex. *J.*
794 *Immunol.* **140**, 3126–3134 (1988).

795 22. Cochran, J. R., Aivazian, D., Cameron, T. O. & Stern, L. J. Receptor clustering and
796 transmembrane signaling in T cells. *Trends Biochem. Sci.* **26**, 304–310 (2001).

797 23. Voon, D. C. *et al.* Use of mRNA- and protein-destabilizing elements to develop a
798 highly responsive reporter system. *Nucleic Acids Res.* **33**, e27 (2005).

799 24. Hall, M. P. *et al.* Engineered luciferase reporter from a deep sea shrimp utilizing a
800 novel imidazopyrazinone substrate. *ACS Chem. Biol.* **7**, 1848–1857 (2012).

801 25. Au-Yeung, B. B. *et al.* A sharp T-cell antigen receptor signaling threshold for T-cell
802 proliferation. *Proc. Natl. Acad. Sci. U. S. A.* **111**, E3679–88 (2014).

803 26. Au-Yeung, B. B. *et al.* IL-2 Modulates the TCR Signaling Threshold for CD8 but Not
804 CD4 T Cell Proliferation on a Single-Cell Level. *J. Immunol.* **198**, 2445–2456
805 (2017).

806 27. Allison, K. A. *et al.* Affinity and dose of TCR engagement yield proportional
807 enhancer and gene activity in CD4+ T cells. *Elife* **5**, (2016).

808 28. Richard, A. C. *et al.* T cell cytolytic capacity is independent of initial stimulation
809 strength. *Nat. Immunol.* **19**, 849–858 (2018).

810 29. Iezzi, G., Karjalainen, K. & Lanzavecchia, A. The duration of antigenic stimulation
811 determines the fate of naive and effector T cells. *Immunity* **8**, 89–95 (1998).

812 30. van Stipdonk, M. J., Lemmens, E. E. & Schoenberger, S. P. Naïve CTLs require a
813 single brief period of antigenic stimulation for clonal expansion and differentiation.
814 *Nat. Immunol.* **2**, 423–429 (2001).
815 31. Schrum, A. G., Palmer, E. & Turka, L. A. Distinct temporal programming of naive
816 CD4+ T cells for cell division versus TCR-dependent death susceptibility by
817 antigen-presenting macrophages. *Eur. J. Immunol.* **35**, 449–459 (2005).
818 32. Eyquem, J. *et al.* Targeting a CAR to the TRAC locus with CRISPR/Cas9 enhances
819 tumour rejection. *Nature* **543**, 113–117 (2017).
820 33. Watanabe, K., Kuramitsu, S., Posey, A. D., Jr & June, C. H. Expanding the
821 Therapeutic Window for CAR T Cell Therapy in Solid Tumors: The Knowns and
822 Unknowns of CAR T Cell Biology. *Front. Immunol.* **9**, 2486 (2018).
823 34. Mohammad, M. P., Munzarová Pondelícková, V., Zeman, J., Gunišová, S. &
824 Valášek, L. S. In vivo evidence that eIF3 stays bound to ribosomes elongating and
825 terminating on short upstream ORFs to promote reinitiation. *Nucleic Acids Res.* **45**,
826 2658–2674 (2017).
827 35. Lin, Y. *et al.* eIF3 associates with 80S ribosomes to promote translation elongation,
828 mitochondrial homeostasis, and muscle health. *bioRxiv* 651240 (2019)
829 doi:10.1101/651240.
830 36. Bohlen, J., Fenzl, K., Kramer, G., Bukau, B. & Teleman, A. A. Selective 40S
831 footprinting reveals that scanning ribosomes remain cap-tethered in human cells.
832 *bioRxiv* 806364 (2019) doi:10.1101/806364.
833 37. Tan, H. *et al.* Integrative Proteomics and Phosphoproteomics Profiling Reveals
834 Dynamic Signaling Networks and Bioenergetics Pathways Underlying T Cell

835 Activation. *Immunity* **46**, 488–503 (2017).

836 38. Myers, D. R., Wheeler, B. & Roose, J. P. mTOR and other effector kinase signals
837 that impact T cell function and activity. *Immunol. Rev.* **291**, 134–153 (2019).

838 39. Manfrini, N. *et al.* High levels of eukaryotic Initiation Factor 6 (eIF6) are required for
839 immune system homeostasis and for steering the glycolytic flux of TCR-stimulated
840 CD4+ T cells in both mice and humans. *Dev. Comp. Immunol.* **77**, 69–76 (2017).

841 40. Corcoran, D. L. *et al.* PARalyzer: definition of RNA binding sites from PAR-CLIP
842 short-read sequence data. *Genome Biol.* **12**, R79 (2011).

843 41. Danan, C., Manickavel, S. & Hafner, M. PAR-CLIP: A Method for Transcriptome-
844 Wide Identification of RNA Binding Protein Interaction Sites. *Methods Mol. Biol.*
845 **1358**, 153–173 (2016).

846 42. Bray, N. L., Pimentel, H., Melsted, P. & Pachter, L. Near-optimal probabilistic RNA-
847 seq quantification. *Nat. Biotechnol.* **34**, 525–527 (2016).

848 43. Cunningham, F. *et al.* Ensembl 2019. *Nucleic Acids Res.* **47**, D745–D751 (2019).

849 44. Szklarczyk, D. *et al.* STRING v11: protein-protein association networks with
850 increased coverage, supporting functional discovery in genome-wide experimental
851 datasets. *Nucleic Acids Res.* **47**, D607–D613 (2019).

852 45. Wickham, H., Chang, W. & Others. ggplot2: Create elegant data visualisations
853 using the grammar of graphics. *R package version* **2**, (2016).

854 46. Martin, M. Cutadapt removes adapter sequences from high-throughput sequencing
855 reads. *EMBnet.journal* **17**, 10–12 (2011).

856 47. Frankish, A. *et al.* GENCODE reference annotation for the human and mouse
857 genomes. *Nucleic Acids Res.* **47**, D766–D773 (2019).

858 48. Love, M. I., Huber, W. & Anders, S. Moderated estimation of fold change and
859 dispersion for RNA-seq data with DESeq2. *Genome Biol.* **15**, 550 (2014).
860 49. Soneson, C., Love, M. I. & Robinson, M. D. Differential analyses for RNA-seq:
861 transcript-level estimates improve gene-level inferences. *F1000Res.* **4**, 1521
862 (2015).
863 50. Zhu, A., Ibrahim, J. G. & Love, M. I. Heavy-tailed prior distributions for sequence
864 count data: removing the noise and preserving large differences. *Bioinformatics* **35**,
865 2084–2092 (2019).
866 51. Schumann, K. *et al.* Generation of knock-in primary human T cells using Cas9
867 ribonucleoproteins. *Proc. Natl. Acad. Sci. U. S. A.* **112**, 10437–10442 (2015).
868 52. Parslow, A., Cardona, A. & Bryson-Richardson, R. J. Sample drift correction
869 following 4D confocal time-lapse imaging. *J. Vis. Exp.* (2014) doi:10.3791/51086.
870 53. Noguchi, S. *et al.* FANTOM5 CAGE profiles of human and mouse samples. *Sci*
871 *Data* **4**, 170112 (2017).

872

873

874 **Extended Data Figures**

875

876 **Extended Data Figure 1. Composition of eIF3 in the Jurkat PAR-CLIP experiments.**
877 **a**, Composition of eIF3 in I+PMA activated and non-activated Jurkat cells after anti-
878 EIF3B immunoprecipitation (IP), identified by mass spectrometry. Shown is an SDS
879 polyacrylamide gel stained with Coomassie Brilliant Blue. **b**, Composition of eIF3 in
880 activated Jurkat cells determined by western blot after anti-EIF3B IP. IN: input; FT: flow-
881 through from anti-EIF3B IP beads; ELU: elution of eIF3 from anti-EIF3B IP beads. Anti-
882 EIF4G1 and anti-RPS19 western blots confirm stringency of bead wash steps[5].

883

884 **Extended Data Figure 2. Categories of RNA crosslinked to eIF3 by PAR-CLIP in**
885 **Jurkat cells.** PAR-CLIP crosslinking sites to eIF3, defined by clusters, divided into RNA
886 categories, in I+PMA activated Jurkat cells (left) and non-activated Jurkat cells (right). In
887 all panels, RNA categories include: 5'-UTR, 5'-UTR of mRNA; 3'-UTR, 3'-UTR of
888 mRNA; CDS, protein coding region of mRNA; Start codon, beginning of mRNA CDS;
889 Stop codon, stop codon region of mRNA; Intron, regions of pre-mRNA; Other, other
890 classes of RNA; No annotation, reads that map to the human genome but that have no
891 annotation assigned. Clusters in different mRNA categories may occur in the same
892 mRNA species.

893

894 **Extended Data Figure 3. Properties of PAR-CLIP sequence reads. a**, The length
895 distribution of PAR-CLIP clusters mapped to RNAs crosslinked to eIF3 in the EIF3A/C/B
896 samples, from activated (left) and non-activated (right) Jurkat cells. **b**, The frequency

897 distribution of eIF3 PAR-CLIP clusters mapped to RNAs in the EIF3A/C/B samples,
898 from activated (left) and non-activated (right) Jurkat cells. In all panels, the distributions
899 are the average of both biological replicates. RNA PAR-CLIP properties observed in the
900 EIF3A/C/B sample are representative of those seen in PAR-CLIP sequence reads of
901 RNAs crosslinked to other eIF3 subunits.
902
903 **Extended Data Figure 4. Comparison of transcription profiles and PAR-CLIP**
904 **reads.** MA plots of **a**, non-activated Jurkat cells compared to Jurkat cells activated with
905 I+PMA for 5 hours (left) and HEK293T cells compared to Jurkat cells activated with
906 I+PMA for 5 hours (right). In **a**, M = $\log_2$(HEK293T mRNA TPM/Jurkat mRNA TPM),
907 and A = mean(TPM) for activated Jurkat mRNAs. TPM, transcripts per million. The FDR
908 was set to 0.01, and the blue dots indicate significant fold changes. **b,** Scatterplot of
909 TPM of mRNAs expressed in activated Jurkat cells (most abundant isoform, see
910 Methods) versus mRNAs identified by PAR-CLIP as crosslinked to eIF3, with ≥ 100 total
911 read counts.
912
913 **Extended Data Figure 5. eIF3-mRNA crosslinking patterns in activated Jurkat**
914 **cells. a**, mRNAs sorted by increasing value of the ratio of normalized 5'-UTR reads to
915 normalized 3'-UTR reads. Values of the ratio of 5'-UTR/3'-UTR normalized reads > 200
916 have been truncated to a value of 200 in the plot (asterisk). The arrow indicates the
917 threshold used to create cumulative plots shown in **Figure 2a**. **b**, Examples of eIF3
918 crosslinking to histone mRNAs *HIST1H2AI* and *HIST1H3H* are shown. Transcription
919 start sites were determined from the FANTOM5 Database[53].

920

921 **Extended Data Figure 6. *TCRA* and *TCRB* mRNA localization patterns. a**, Single
922 plane image of TetraSpeck microspheres (100 nm) adjacent to Jurkat cell probed for P
923 bodies (far left). Scatter plots of pixel intensities in different emission channels are
924 shown: channel 1, 670 nm; channel 2, 570 nm; channel 3, 488 nm. Plots left to right are:
925 channel 1 vs. channel 2, channel 1 vs. channel 3, and channel 2 vs. channel 3. **b**,
926 Single plane image of Jurkat cell probed for *TCRA* mRNA (channel 1), *TCRB* mRNA
927 (channel 2), and DCP1 to mark P bodies (channel 3). Scatter plots to the right are
928 shown as in **a**. **c**, Single plane image and scatter plots for TetraSpeck microspheres as
929 in **a**, but adjacent to Jurkat cell probed for stress granules. **d**, Single plane image of
930 Jurkat cell probed for *TCRA* mRNA (channel 1), *TCRB* mRNA (channel 2), and G3BP1
931 to mark stress granules (channel 3). Scatter plots to the right are shown as in **a**.

932

933 **Extended Data Figure 7. CRISPR/Cas9 RNP mediated genome editing at the *TCRA***
934 **and *TCRB* genomic loci in primary human T cells. a**, Location of gRNA sites
935 targeting the *TCRA* 3'-UTR, to generate *TCRA* Δ*PAR* cells. In *TCRA*, gRNA1 and
936 gRNA2 target hg38 genomic locations chr14:22,551,700 and chr14:22,552,073,
937 respectively. **b**, PCR primers flanking the *TCRA* editing sites. **c**, Analysis of *TCRA* 3'-
938 UTR PAR-CLIP site deletion efficiency. Total genomic DNA extracted from WT, *TCRA*
939 Δ*PAR, TCRB* Δ*PAR* (here serving as a negative control), scrambled gRNA
940 nucleofected (S) and non-nucleofected (N) cells was analyzed by PCR to measure the
941 editing efficiency. *TCRA* Δ*PAR* cells produced a 1283 bp PCR product compared to
942 1676 bp in S, N or *TCRB* Δ*PAR* cells. **d**, Location of gRNA sites of targeting the *TCRB*

943 3'-UTR, to generate *TCRB* Δ*PAR* cells. In *TCRB*, gRNA1 and gRNA2 target hg38
944 genomic locations chr7:142,802,561 and chr7:142,802,695. **e**, PCR primers flanking
945 the *TCRB* editing sites. **f**, Analysis of *TCRB* 3'-UTR PAR-CLIP site deletion efficiency.
946 Total genomic DNA extracted from WT, *TCRA* Δ*PAR* (here serving as a negative
947 control), *TCRB* Δ*PAR*, scrambled gRNA nucleofected (S) and non-nucleofected (N)
948 cells were analyzed by PCR to measure the editing efficiency. *TCRB* Δ*PAR* cells
949 produced a 1022 bp PCR product compared to 1190 bp in S, N or *TCRA* Δ*PAR* cells.
950

951 **Extended Data Figure 8. TCR levels on the cell surface of primary human T cells.**
952 **a**, Percentage of cells expressing TCR on the cell surface measured by flow cytometric
953 analysis (*n* = *2* donors). TCR expressing cells in the cell populations tested: *1gB*, *TCRB*
954 gRNA 1; *2gB*, *TCRB* gRNA 2; *1+2 gB*, *TCRB* gRNA 1+2 (i.e. *TCRB* Δ*PAR*); *1gA*, *TCRA*
955 gRNA 1; *2gA*, *TCRA* gRNA 2; *1+2 gA*, *TCRA* gRNA 1+2 (i.e. *TCRA* Δ*PAR*); Δ*TCR*,
956 TCR gRNA targeting the CDS of *TCRA*; *N*, Non-nucleofected cells; SC, Scrambled
957 gRNA. (*n* = 2 donors, with standard deviation shown.) Left: I+PMA activated T cells,
958 after 3 hours of activation; Right: non-activated T cells. P values for *TCRA* Δ*PAR*, *TCRB*
959 Δ*PAR,* Δ*TCR* were < 0.0001 relative to SC in both activated and non-activated cells,
960 using one-way ANOVA. The P values for single guide edited non-activated cells relative
961 to SC were not significant, while in activated cells P = 0.02 – 0.05 relative to SC. **b,**
962 Representative density plots showing the percentage of TCR on the cell surface in non
963 activated T cells for one of the two donors. The cell lines shown are: *TCRA* Δ*PAR*,
964 *TCRB* Δ*PAR*, Δ*TCR* (negative control), and SC.
965

966 **Extended Data Figure 9. Gating strategy for flow cytometric analysis of CD69 and**
967 **CD25 levels.** Primary human T cells were gated to isolate lymphocytes, followed by
968 isolation of single cells, then live cells. Next, cells were gated to separate CD4+ and
969 CD8+ cells expressing T cell activation markers CD69 and CD25 after activation with
970 anti-CD3/anti-CD28 antibodies. Shown is the workflow of the FACS gating, with an
971 example of T cells activated with anti-CD3/anti-CD28 antibodies for 8 hours.
972
973 **Extended Data Figure 10. Phenotypic analysis of CD8+ primary human T cells**
974 **with eIF3 3'-UTR PAR-CLIP sites deleted.** Flow cytometric analysis of CD8+ T cells,
975 showing quantification of T cell activation markers CD69 (early activation marker) and
976 CD25 (mid-activation marker) after activation with anti-CD3/anti-CD28 antibodies at
977 different time points, for all cell populations tested: *1gB*, *TCRB* gRNA 1; *2gB*, *TCRB*
978 gRNA 2; *1+2 gB*, *TCRB* gRNA 1+2 (i.e. *TCRB* Δ*PAR*); *1gA*, *TCRA* gRNA 1; *2gA*, *TCRA*
979 gRNA 2; *1+2 gA*, *TCRA* gRNA 1+2 (i.e. *TCRA* Δ*PAR*); *ΔTCR* gRNA targeting the CDS
980 of *TCRA*; N, Non-nucleofected cells; SC, Scrambled gRNA. ($n = 2$ donors, with mean
981 and standard deviation shown). P values for *TCRA* Δ*PAR*, *TCRB* Δ*PAR,* Δ*TCR* were <
982 0.0001 relative to SC, while single gRNA edited cell lines had P < 0.0001 to P < 0.01,
983 relative to SC as calculated by two-way ANOVA.
984
985 **Extended Data Figure 11. Phenotypic analysis of CD4+ primary human T cells**
986 **with eIF3 3'-UTR PAR-CLIP sites deleted. a**, Flow cytometric analysis of CD4+ T
987 cells, showing quantification of T cell activation markers CD69 (early activation marker)
988 and CD25 (mid-activation marker) after activation with anti-CD3/anti-CD28 antibodies at

989 different time points, for all cell populations tested: *1gB*, *TCRB* gRNA 1; *2gB*, *TCRB*
990 gRNA 2; *1+2 gB*, *TCRB* gRNA 1+2 (i.e. *TCRB* Δ*PAR*); *1gA*, *TCRA* gRNA 1; *2gA*, *TCRA*
991 gRNA 2; *1+2 gA*, *TCRA* gRNA 1+2 (i.e. *TCRA* Δ*PAR*); *ΔTCR* gRNA targeting the CDS
992 of *TCRA*; N, Non-nucleofected cells; SC, Scrambled gRNA. (*n* = *2* donors, with mean
993 and standard deviation shown). P values for *TCRA* Δ*PAR*, *TCRB* Δ*PAR,* Δ*TCR* were <
994 0.0001 relative to SC, while single gRNA edited cell lines had P < 0.0001 to P < 0.01,
995 relative to SC as calculated by two-way ANOVA. **b**, Representative density plots
996 showing the percentage of cells expressing CD69, CD69 and CD25 or CD25 only, for
997 one of two donors. The cell lines shown are *TCRA* Δ*PAR*, *TCRB* Δ*PAR*, Δ*TCR*
998 (negative control), and SC.
999
1000 **Extended Data Figure 12. Cytokine secretion profile of primary human T cells with**
1001 **with eIF3 3'-UTR PAR-CLIP sites deleted .** Quantification of **a**, secreted IL2 and **b,**
1002 secreted IFNγ, for all cell populations tested, as determined by ELISA. Cell populations
1003 tested were: *1gB*, *TCRB* gRNA 1; *2gB*, *TCRB* gRNA 2; *1+2 gB*, *TCRB* gRNA 1+2 (i.e.
1004 *TCRB* Δ*PAR*); *1gA*, *TCRA* gRNA 1; *2gA*, *TCRA* gRNA 2; *1+2 gA*, *TCRA* gRNA 1+2 (i.e.
1005 *TCRA* Δ*PAR*); *ΔTCR* gRNA targeting the CDS of *TCRA*; N, Non-nucleofected cells; SC,
1006 Scrambled gRNA. (*n* = *2* donors, with mean and standard deviation shown.) P values
1007 for *TCRA* Δ*PAR*, *TCRB* Δ*PAR,* Δ*TCR* were < 0.0001 relative to SC, while single gRNA
1008 edited cell lines had P < 0.0001 to P < 0.01, relative to SC as calculated by two-way
1009 ANOVA.
1010

1011 **Extended Data Figure 13. TCR protein and RNA levels in Jurkat cells with eIF3 3'-**
1012 **UTR PAR-CLIP sites deleted. a**, Western blots measuring TCRA protein levels as a
1013 function of time after anti-CD3/anti-CD28 activation. Cell lines are indicated by transcript
1014 structure above the western blots. HSP90 was used as a loading control. **b**, *TCRA* and
1015 *TCRB* mRNA levels in WT Jurkat cells, or Jurkat cells with the *TCRA* eIF3 3'-UTR PAR-
1016 CLIP site deleted, as determined by qRT-PCR at different time points after anti-
1017 CD3/anti-CD28 activation. **c**, *TCRA* and *TCRB* mRNA levels in WT Jurkat cells, or
1018 Jurkat cells with the *TCRB* eIF3 3'-UTR PAR-CLIP site deleted, as determined by qRT-
1019 PCR at different time points after anti-CD3/anti-CD28 activation. (n = 2, with mean ±
1020 standard deviations shown), **** P < 0.0001, *** P < 0.001, ** P < 0.01 for *TCRA* Δ*PAR*
1021 or *TCRB* Δ*PAR* relative to WT, using two-way ANOVA.
1022
1023 **Extended Data Figure 14. TCR mRNA binding to eIF3 in Jurkat cells.**
1024 Immunoprecipitation of eIF3 using an anti-EIF3B antibody[5] , followed by qRT-PCR to
1025 quantify the amount of **a**, *TCRA* or **b**, *TCRB* mRNA bound to eIF3. Jurkat cells with or
1026 without the eIF3 PAR-CLIP site in the 3'-UTR were analyzed after activation with anti-
1027 CD3/anti-CD28 antibodies for 5 hours (left) and 8 hours (right). Percent mRNA bound to
1028 anti-EIF3B beads relative to total mRNA isolated from the cells (*TCRA* or *TCRB* on the
1029 left, *IL2* on the right). (n = 3, with mean and standard deviations shown). For *TCRA* and
1030 *TCRB* mRNAs, P < 0.0001 relative to WT. P values for IL2 mRNAs for Δ*PAR* relative
1031 to WT were not significant using two-way ANOVA. The schematic of the experiment is
1032 shown in **Figure 5d**.
1033

1034 **Extended Data Figure 15. TCR clustering in Jurkat cells.** WT, *TCRA* Δ*PAR, TCRB*
1035 Δ*PAR* cells exhibiting TCR clustering, as determined using anti-TCRA/anti-TCRB
1036 protein staining and Airyscan confocal microscopy. Cells were activated with anti-
1037 CD3/anti-CD28 antibodies for 5 hours (left) and 8 hours (right). (*n = 5* for each time
1038 point after activation for all cell lines, with representative images shown)
1039
1040 **Extended Data Figure 16. Phenotypic analysis of Jurkat cells. a**, Flow cytometric
1041 analysis of cells expressing T cell activation markers CD69 (early activation marker) and
1042 CD25 (mid-activation marker) in WT, *TCRA* Δ*PAR* or *TCRB* Δ*PAR* Jurkat cells at
1043 different time points after stimulation with anti-CD3/anti-CD28 antibodies. (*n* = 3, with
1044 mean and standard deviations shown). Left graph, $P < 0.0001$ for CD69 expression in
1045 *TCRA* Δ*PAR* and *TCRB* Δ*PAR* cells relative to WT cells using one-way ANOVA. Right
1046 graph, $P < 0.001$ for CD69 and CD25 expression of *TCRA* Δ*PAR* and *TCRB* Δ*PAR*
1047 relative to WT using two-way ANOVA. **b**, Density plots showing cell populations
1048 expressing CD69+ only, CD69+ CD25+ or CD25+ only from WT, *TCRA* Δ*PAR* or *TCRB*
1049 Δ*PAR* Jurkat cells at different time points after stimulation with anti-CD3/anti-CD28
1050 antibodies, (*n = 3*, with representative plots shown). (**c**) Quantification of secreted IL2
1051 from WT, *TCRA* Δ*PAR* or *TCRB* Δ*PAR* cells at different time points after stimulation
1052 with anti-CD3/anti-CD28 antibodies, as determined by ELISA. (*n* = 3, with mean and
1053 standard deviation shown.) $P < 0.0001$ for *TCRA* Δ*PAR* and *TCRB* Δ*PAR* cells relative
1054 to WT cells, as determined by two-way ANOVA.
1055
1056

1057 **Supplementary Information**

1058 Supplementary Figures 1-3: Raw images of gels used for Fig. 1b, Fig. 3a, Extended
1059 Data Fig. 1, and Extended Data Fig. 13a.

1060

1061 Supplementary Table 1: Subunits in eIF3 crosslinked to RNA in activated Jurkat cells.
1062 Lists the eIF3 subunits, percent sequence coverage and number of identified peptides.

1063

1064 Supplementary Table 2: PARpipe statistics for eIF3 PAR-CLIP samples. Samples are
1065 indexed in the first tab, including both biological replicates for activated and non-
1066 activated Jurkat cells. Statistics are given for each library at the read, cluster and group
1067 level.

1068

1069 Supplementary Table 3: PAR-CLIP mapping to individual genes for each eIF3 PAR-
1070 CLIP sample. Samples are indexed in the first tab, including both biological replicates
1071 for activated and non-activated Jurkat cells. First lists the gene name and number of
1072 clusters identified. The statistics also include: Sum, sum of that statistic over all sites for
1073 that gene; Med, median of that statistic for all sites for that gene; ReadCount, total reads
1074 mapping to the gene; T2Cfraction, number of reads with T-to-C conversions / number of
1075 reads; ConversionSpecificity, log(number of reads with T-to-C conversions / number of
1076 reads with other conversions); UniqueReads, reads collapsed to single copies. Also
1077 included: 5'utr/Intron/Exon/3'utr/Start_codon/Stop_codon, number of sites mapping to
1078 that annotation category; Junction, number of sites mapping to a junction between

1079 categories (coding-intron, coding-3'utr, etc.); GeneType, as described in the gene_type
1080 category for this gene in the .gtf file used.
1081
1082 Supplementary Table 4. Transcriptome analysis of HEK293T cells and non-activated or
1083 activated Jurkat cells. Each tab lists transcript name and version, gene name, type of
1084 transcript, length of transcript, and mean transcripts per million, calculated from two
1085 biological replicates.
1086
1087 Supplementary Table 5. Differential expression analysis of HEK293T or non-activated
1088 vs. activated Jurkat cells. Each tab lists the gene name, mean of normalized counts,
1089 log_2-fold change, log_2-fold change standard error, Wald statistic, Wald test P-value, and
1090 Benjamini-Hochberg adjusted P-value.
1091
1092 Supplementary Table 6. Pathway enrichment analysis. Lists for both biological
1093 replicates of the EIF3A/C/B PAR-CLIP libraries are included (genes with >= 100 reads),
1094 along with associated transcript names, lengths in nts of the 5'-UTR, coding region, and
1095 3'-UTR, and reads normalized to the lengths of the transcript regions. Tabs also include
1096 the top tissue-specific pathway enrichment categories determined using the STRING
1097 Database. These list: the Gene Ontology (GO) number, GO description, observed gene
1098 count, background gene count, false discovery rate, and matching proteins in the
1099 network by Ensembl protein ID, and by gene name.
1100

1101 Supplementary Table 7. Reagent information for experiments. Lists include antibodies

1102 used, PCR primers, qPCR primers, gRNA targeting sequences, and FISH probes.

Figure 1

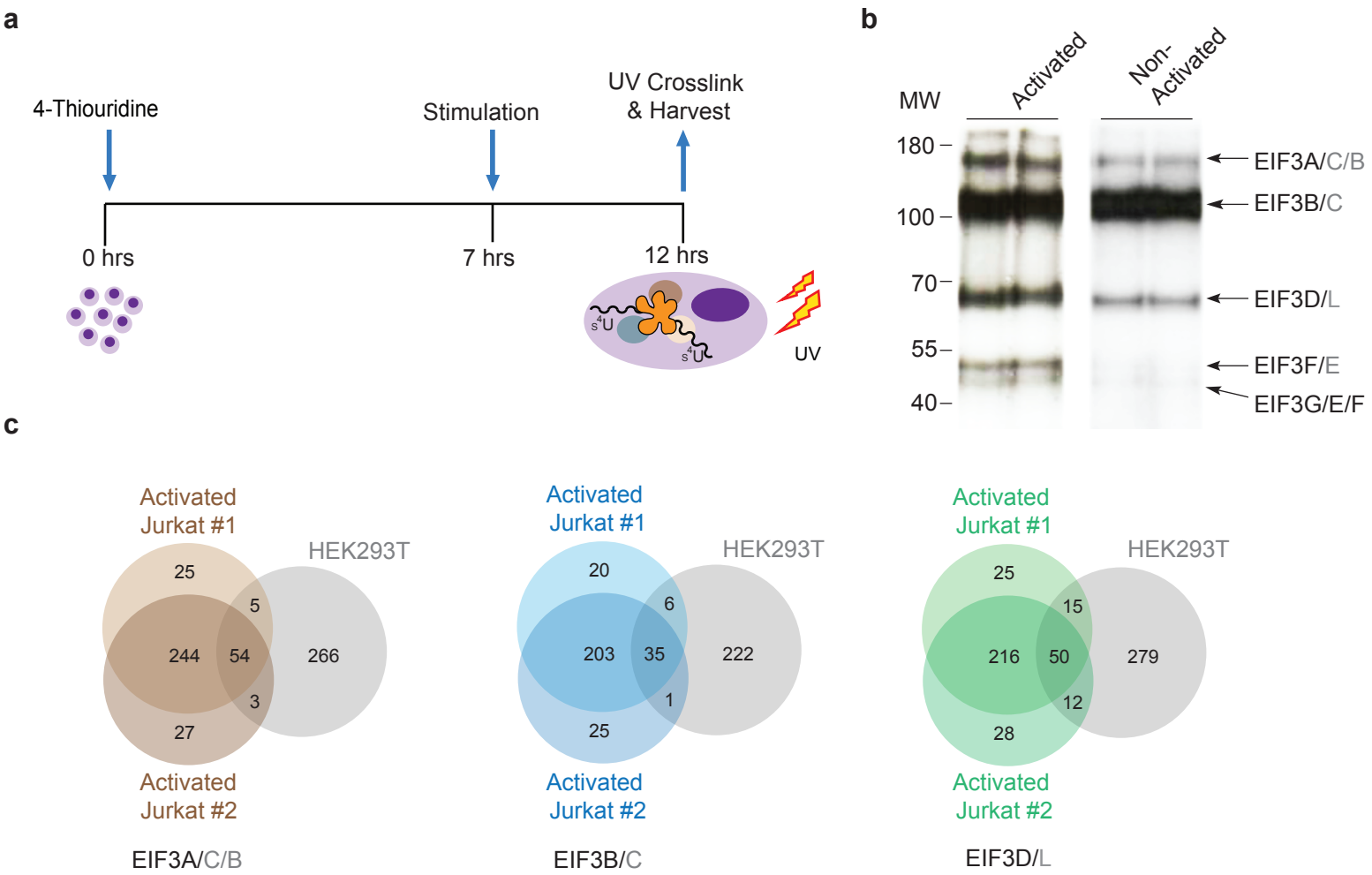
a
4-Thiouridine
Stimulation
UV Crosslink
& Harvest
0 hrs
7 hrs
12 hrs
UV
b
MW
Activated
Non-
Activated
180
100
70
55
40
EIF3A/C/B
EIF3B/C
EIF3D/L
EIF3F/E
EIF3G/E/F
c
Activated
Jurkat #1
HEK293T
Activated
Jurkat #2
25
5
244
54
266
3
27
EIF3A/C/B
Activated
Jurkat #1
HEK293T
Activated
Jurkat #2
20
6
203
35
222
1
25
EIF3B/C
Activated
Jurkat #1
HEK293T
Activated
Jurkat #2
25
15
216
50
279
12
28
EIF3D/L

Figure 2

a

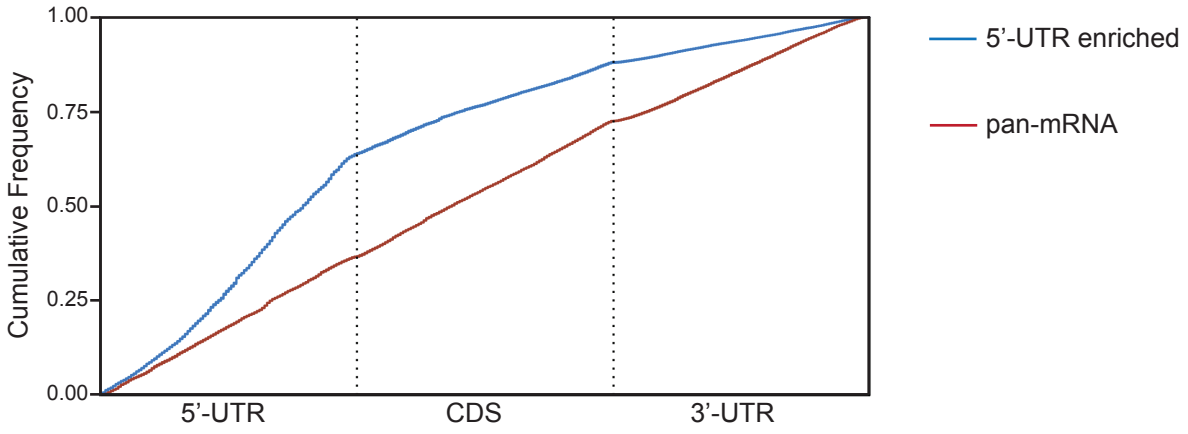
Cumulative Frequency
1.00
0.75
0.50
0.25
0.00
5'-UTR
CDS
3'-UTR
5'-UTR enriched
pan-mRNA

b

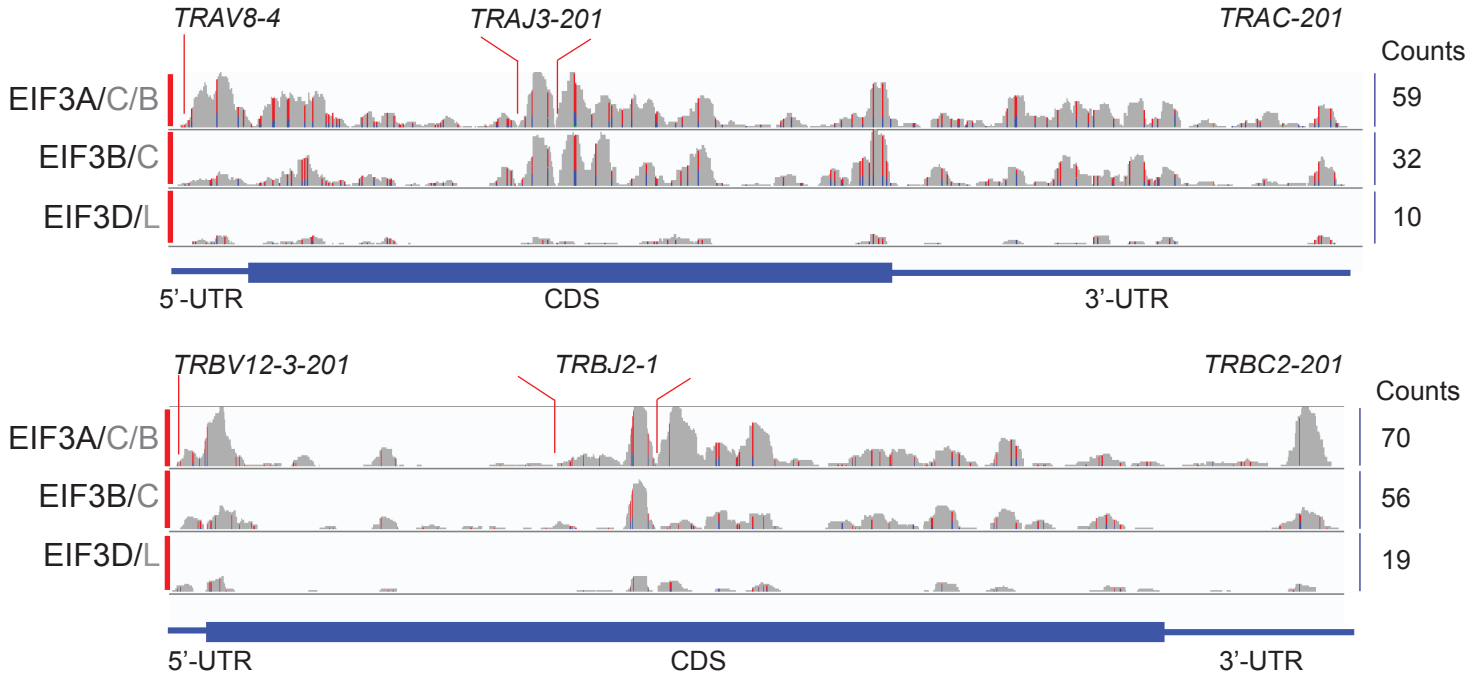
TRAV8-4
TRAJ3-201
TRAC-201
Counts
EIF3A/C/B
EIF3B/C
EIF3D/L
59
32
10
5'-UTR
CDS
3'-UTR
TRBV12-3-201
TRBJ2-1
TRBC2-201
Counts
EIF3A/C/B
EIF3B/C
EIF3D/L
70
56
19
5'-UTR
CDS
3'-UTR

c

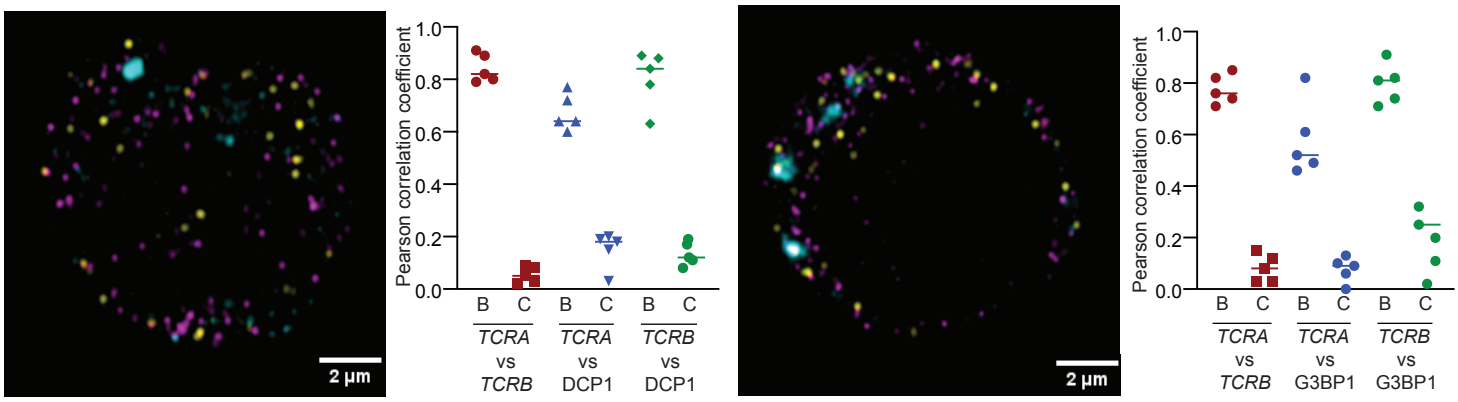
2 µm
Pearson correlation coefficient
1.0
0.8
0.6
0.4
0.2
0.0
B C B C B C
TCRA vs TCRB
TCRA vs DCP1
TCRB vs DCP1
2 µm
Pearson correlation coefficient
B C B C B C
TCRA vs TCRB
TCRA vs G3BP1
TCRB vs G3BP1

Figure 3

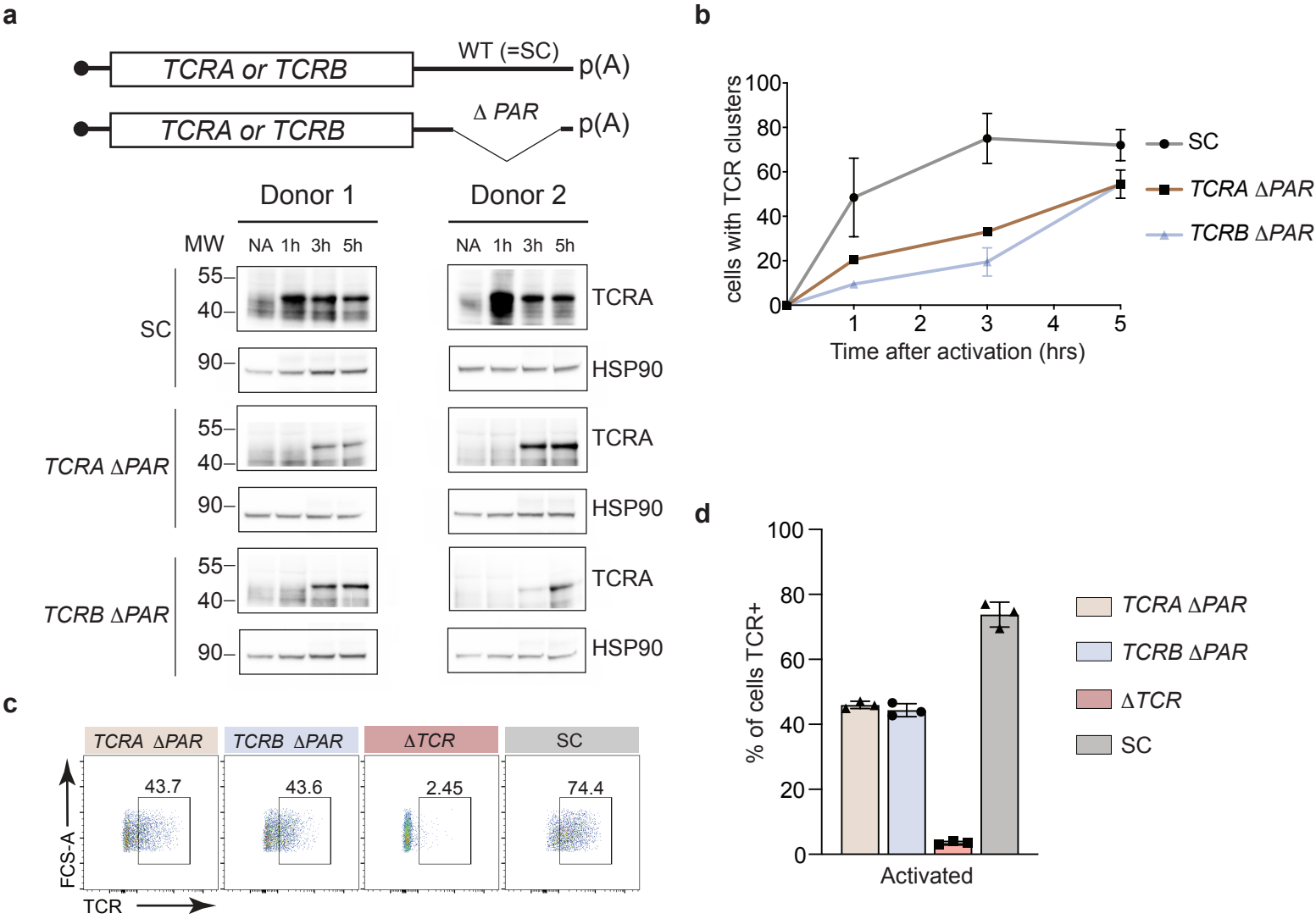
a
TCRA or TCRB
WT (=SC)
p(A)
TCRA or TCRB
Δ PAR
p(A)
Donor 1
Donor 2
MW
NA 1h 3h 5h
NA 1h 3h 5h
55
40
90
SC
TCRA ΔPAR
TCRB ΔPAR
TCRA
HSP90
b
cells with TCR clusters
Time after activation (hrs)
SC
TCRA ΔPAR
TCRB ΔPAR
c
TCRA ΔPAR
TCRB ΔPAR
ΔTCR
SC
43.7
43.6
2.45
74.4
FCS-A
TCR
d
% of cells TCR+
Activated
TCRA ΔPAR
TCRB ΔPAR
ΔTCR
SC

Figure 4

a

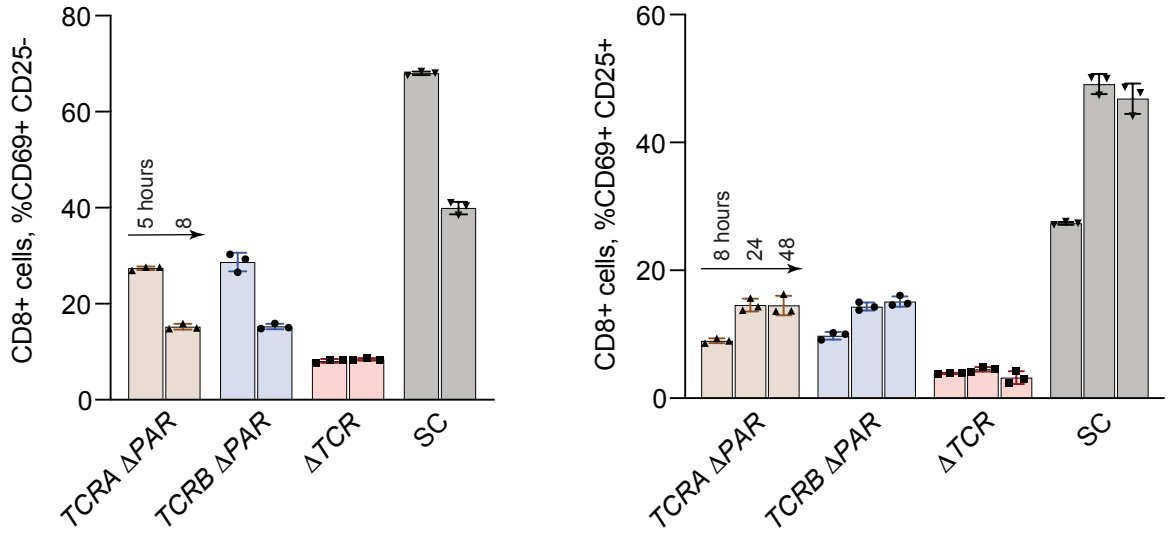
CD8+ cells, %CD69+ CD25-
80
60
40
20
0
5 hours
8
TCRA ΔPAR
TCRB ΔPAR
ΔTCR
SC
CD8+ cells, %CD69+ CD25+
60
40
20
0
8 hours
24
48
TCRA ΔPAR
TCRB ΔPAR
ΔTCR
SC

b

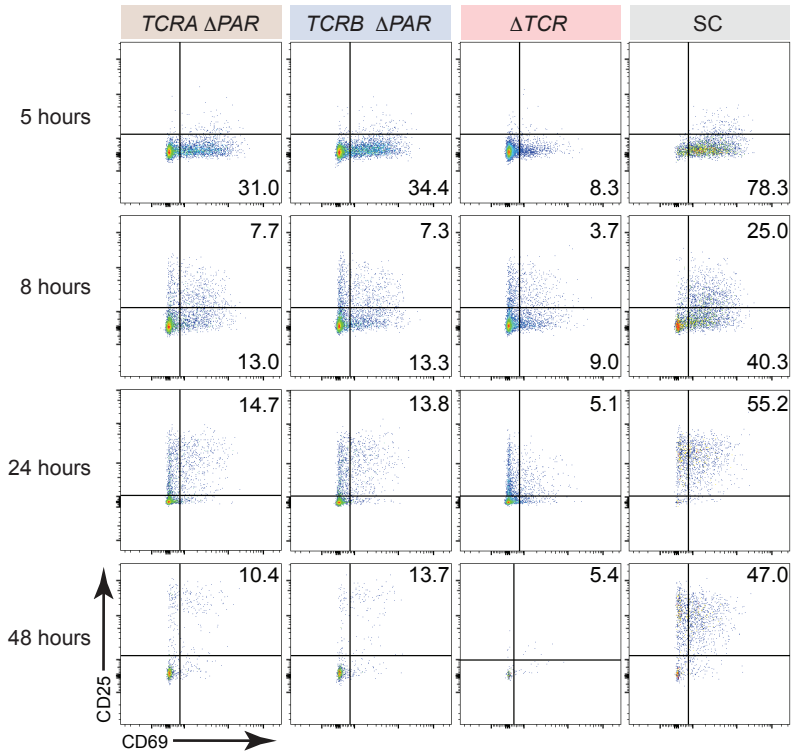
TCRA ΔPAR
TCRB ΔPAR
ΔTCR
SC
5 hours
31.0
34.4
8.3
78.3
8 hours
7.7
7.3
3.7
25.0
13.0
13.3
9.0
40.3
24 hours
14.7
13.8
5.1
55.2
48 hours
10.4
13.7
5.4
47.0
CD25
CD69

c

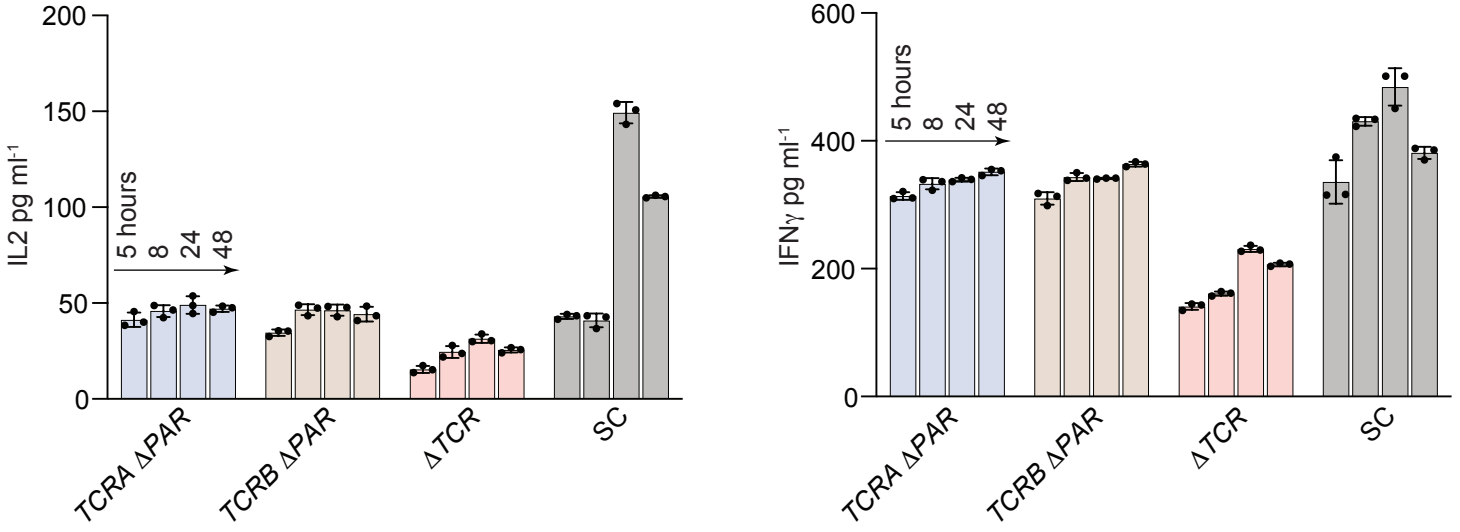
IL2 pg ml-1
200
150
100
50
0
5 hours
8
24
48
TCRA ΔPAR
TCRB ΔPAR
ΔTCR
SC
IFNγ pg ml-1
600
400
200
0
5 hours
8
24
48
TCRA ΔPAR
TCRB ΔPAR
ΔTCR
SC

Figure 5

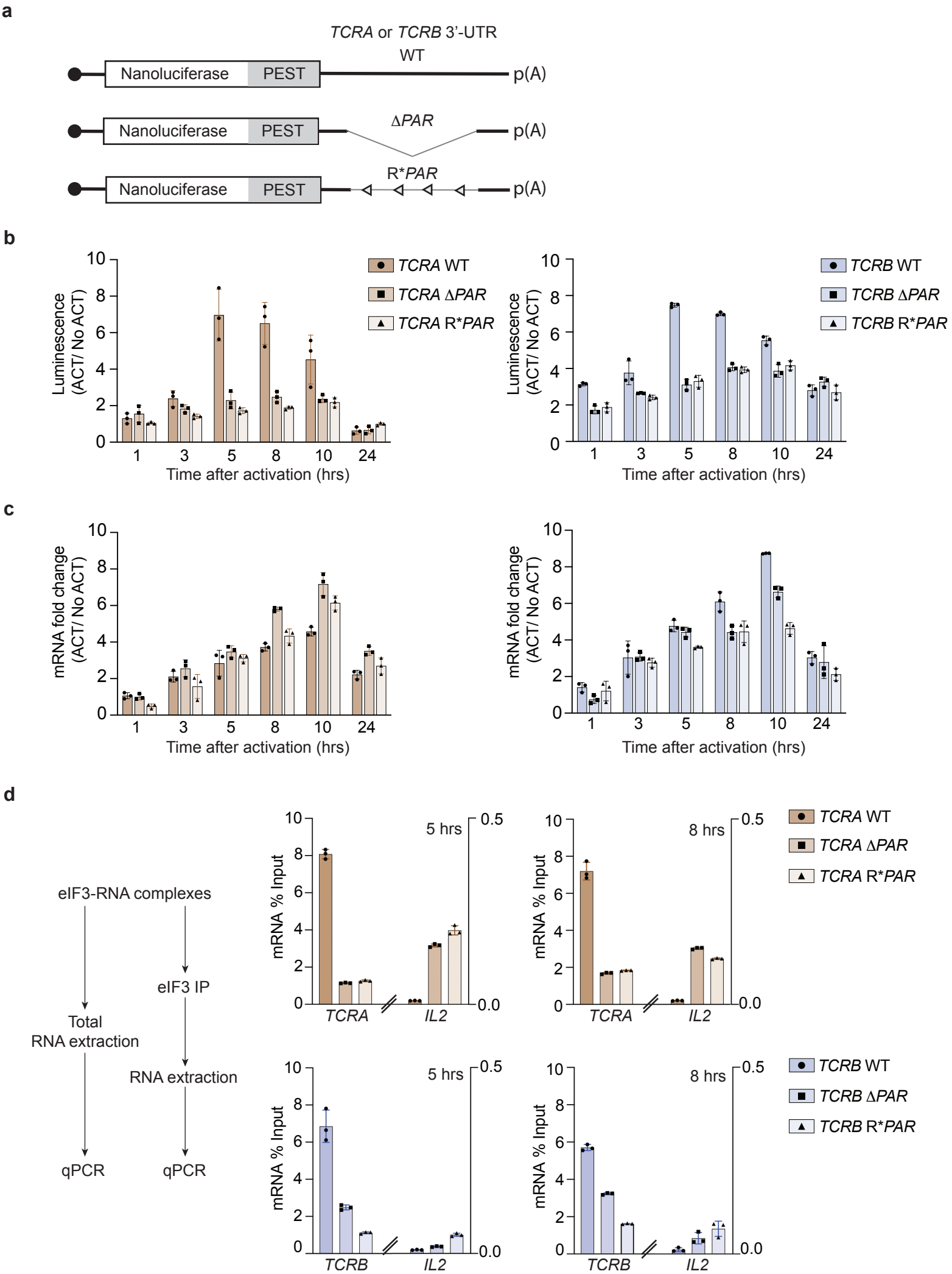
a
TCRA or TCRB 3'-UTR
WT
Nanoluciferase
PEST
p(A)
ΔPAR
R*PAR
b
Luminescence (ACT/ No ACT)
Time after activation (hrs)
TCRA WT
TCRA ΔPAR
TCRA R*PAR
TCRB WT
TCRB ΔPAR
TCRB R*PAR
c
mRNA fold change (ACT/ No ACT)
d
eIF3-RNA complexes
eIF3 IP
Total RNA extraction
RNA extraction
qPCR
mRNA % Input
5 hrs
8 hrs
TCRA
IL2
TCRB

Extended Data Fig. 1

a

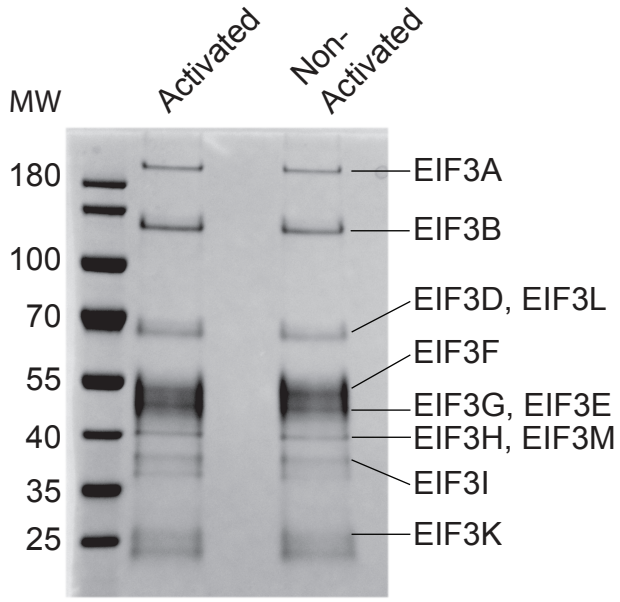

b

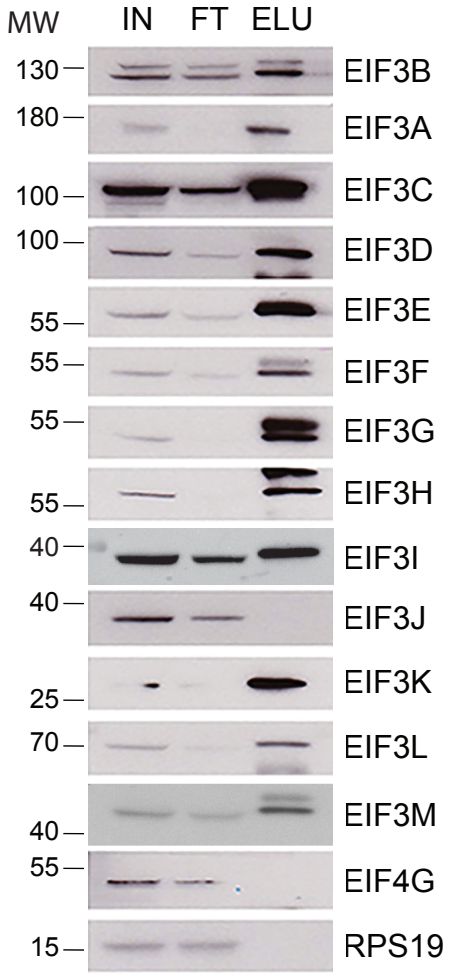

Extended Data Fig. 2

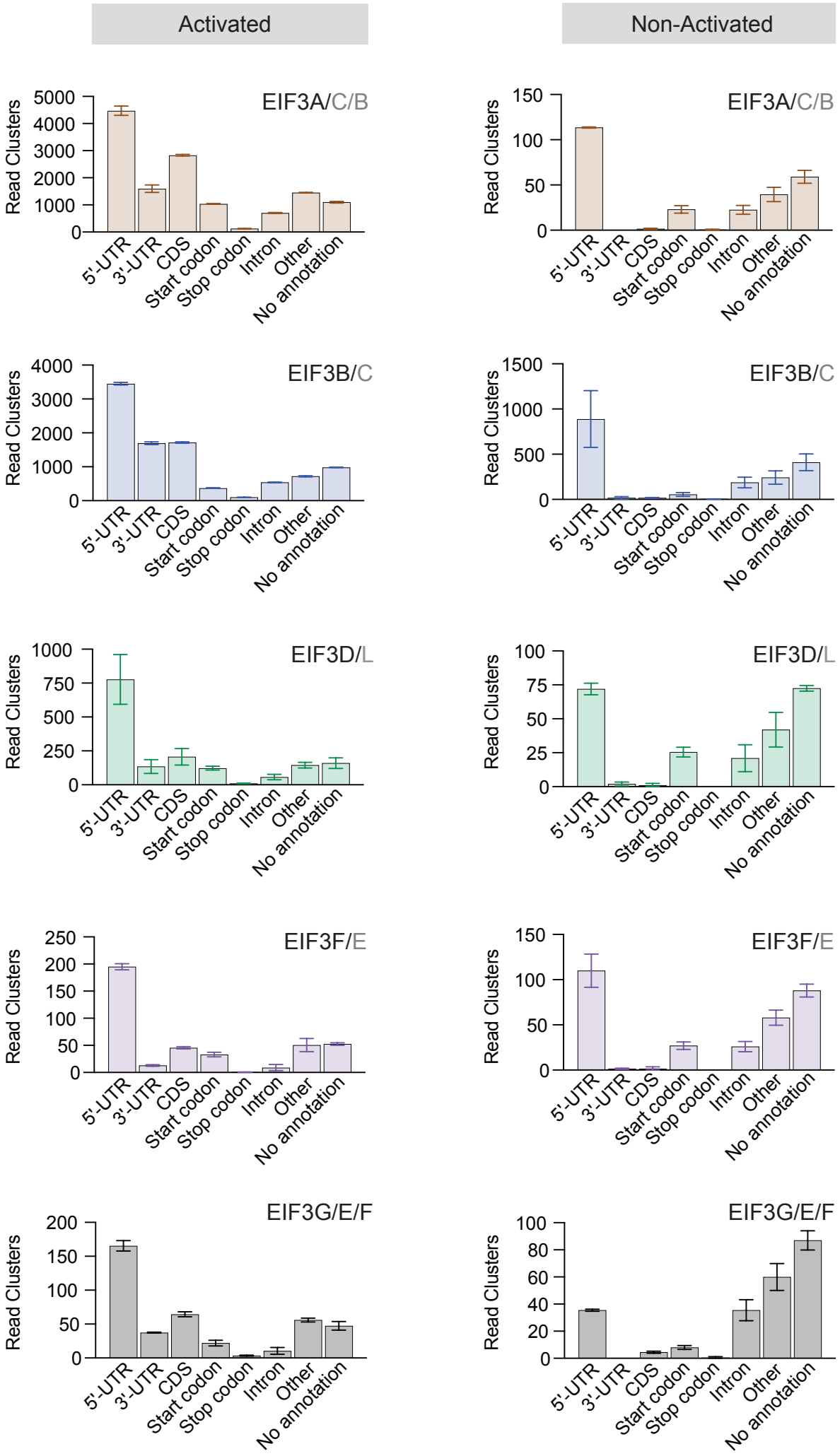

Extended Data Fig. 3

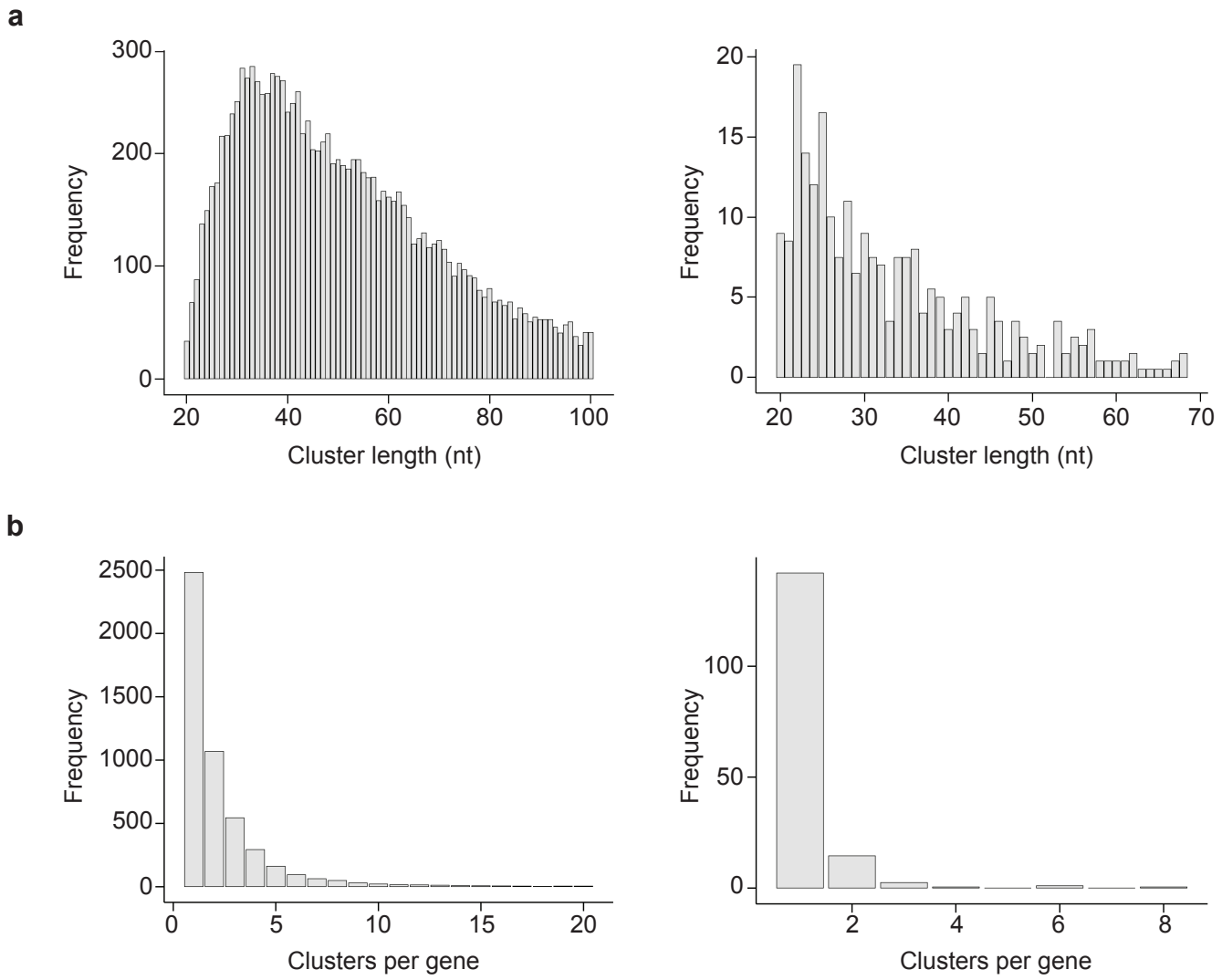

Extended Data Fig. 4

a

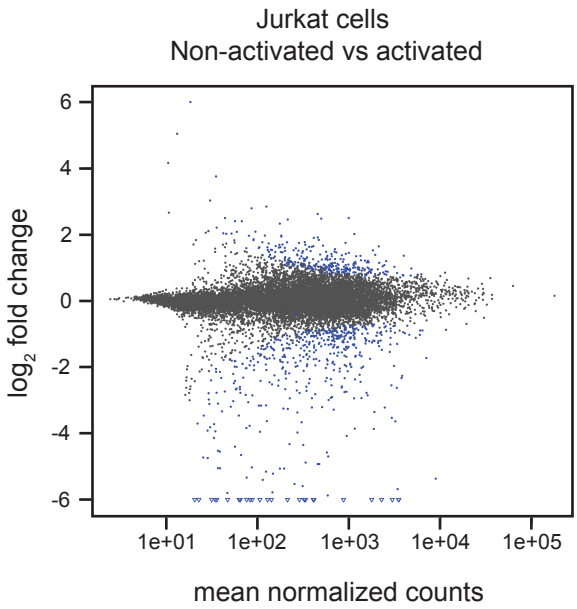

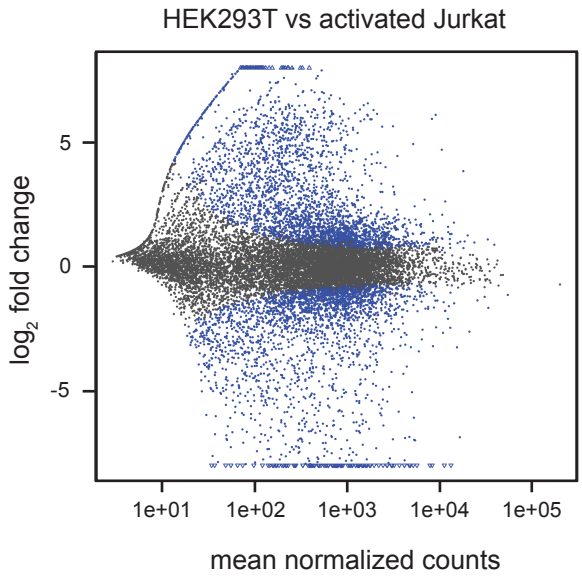

b

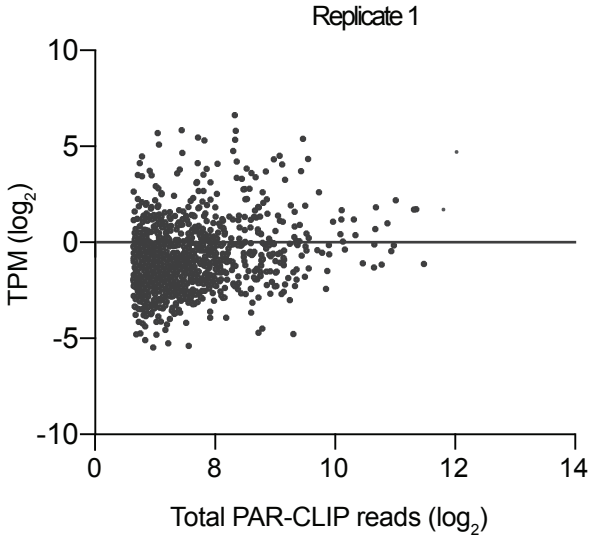

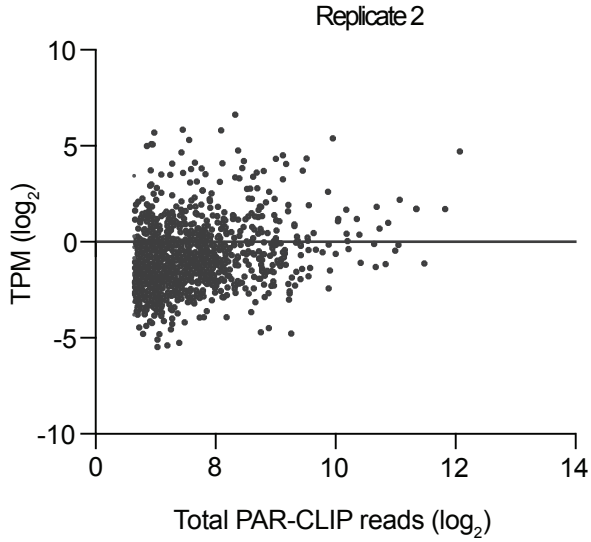

Extended Data Fig. 5

a

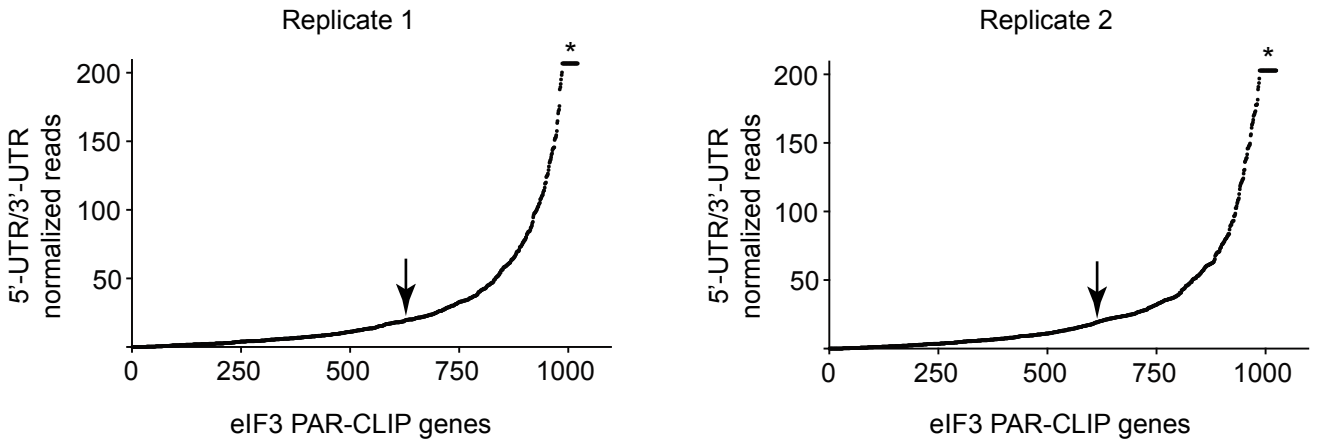

b

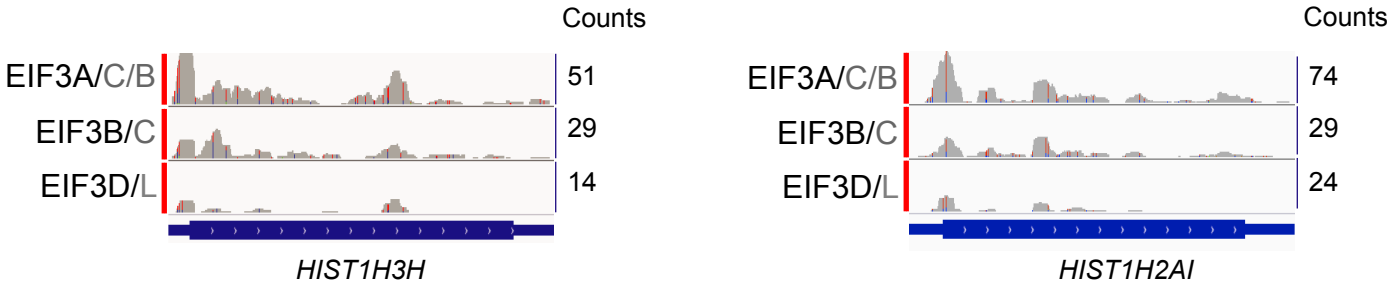

Extended Data Fig. 6

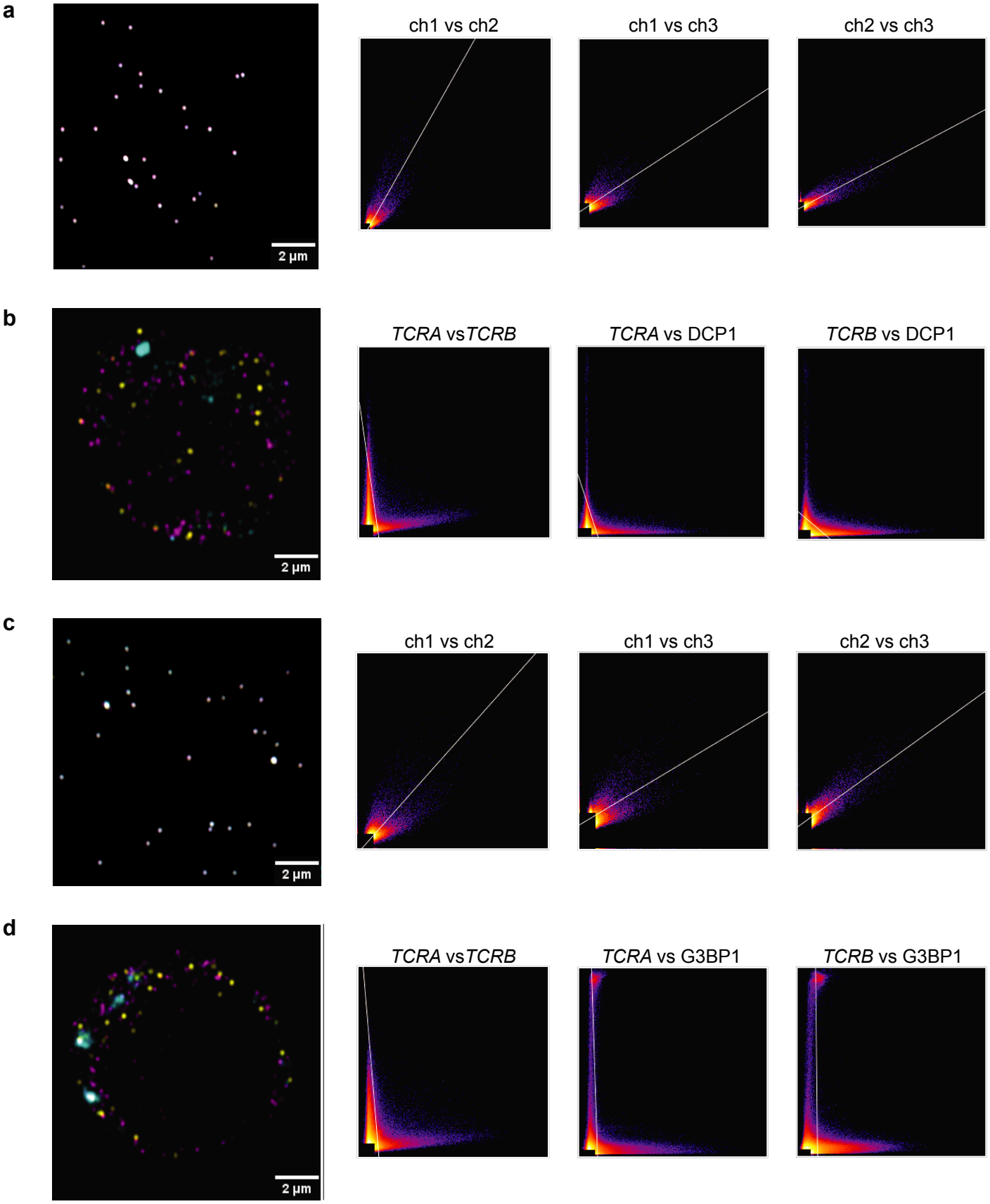

Extended Data Fig. 7

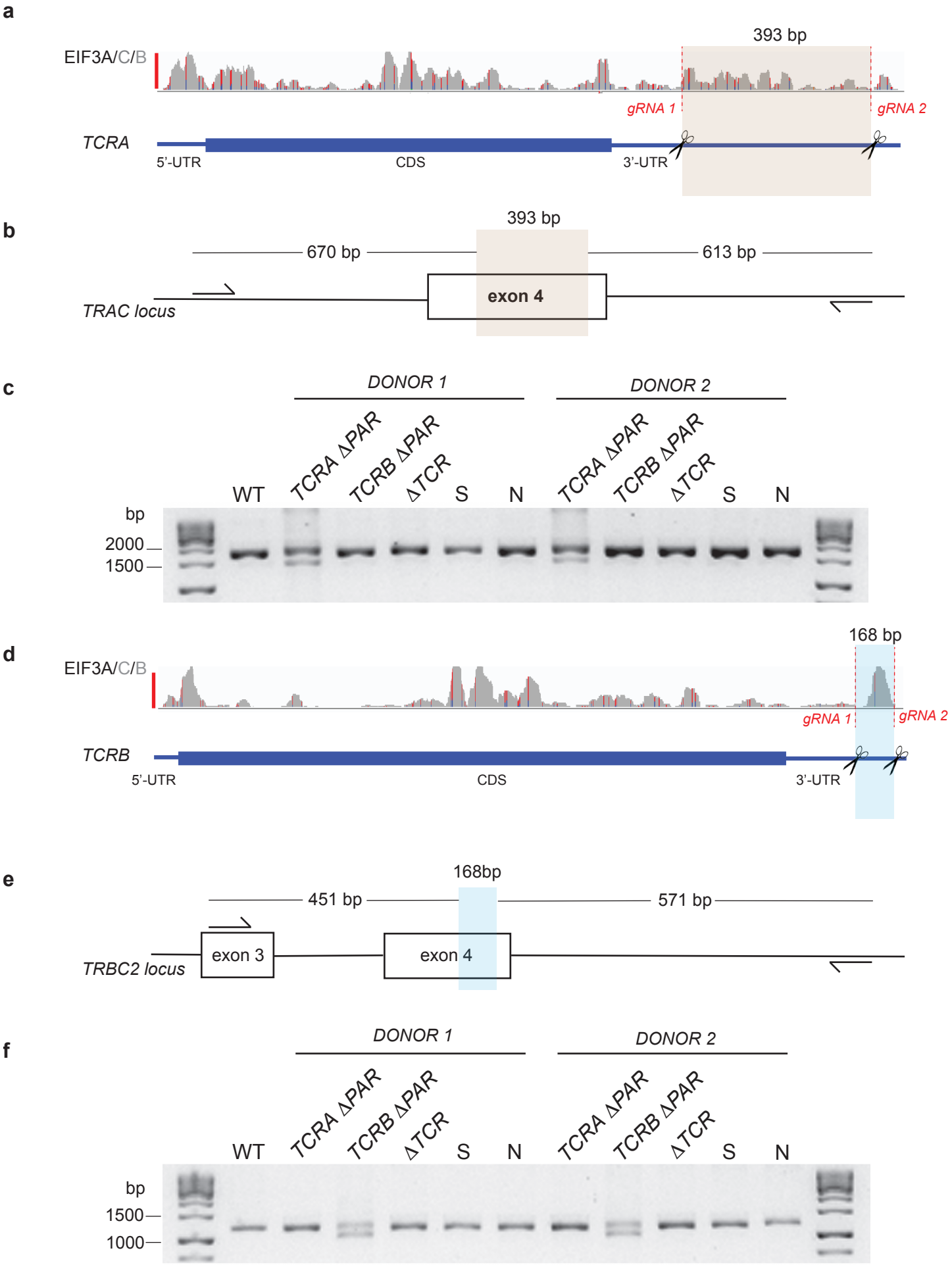

Extended Data Fig. 8

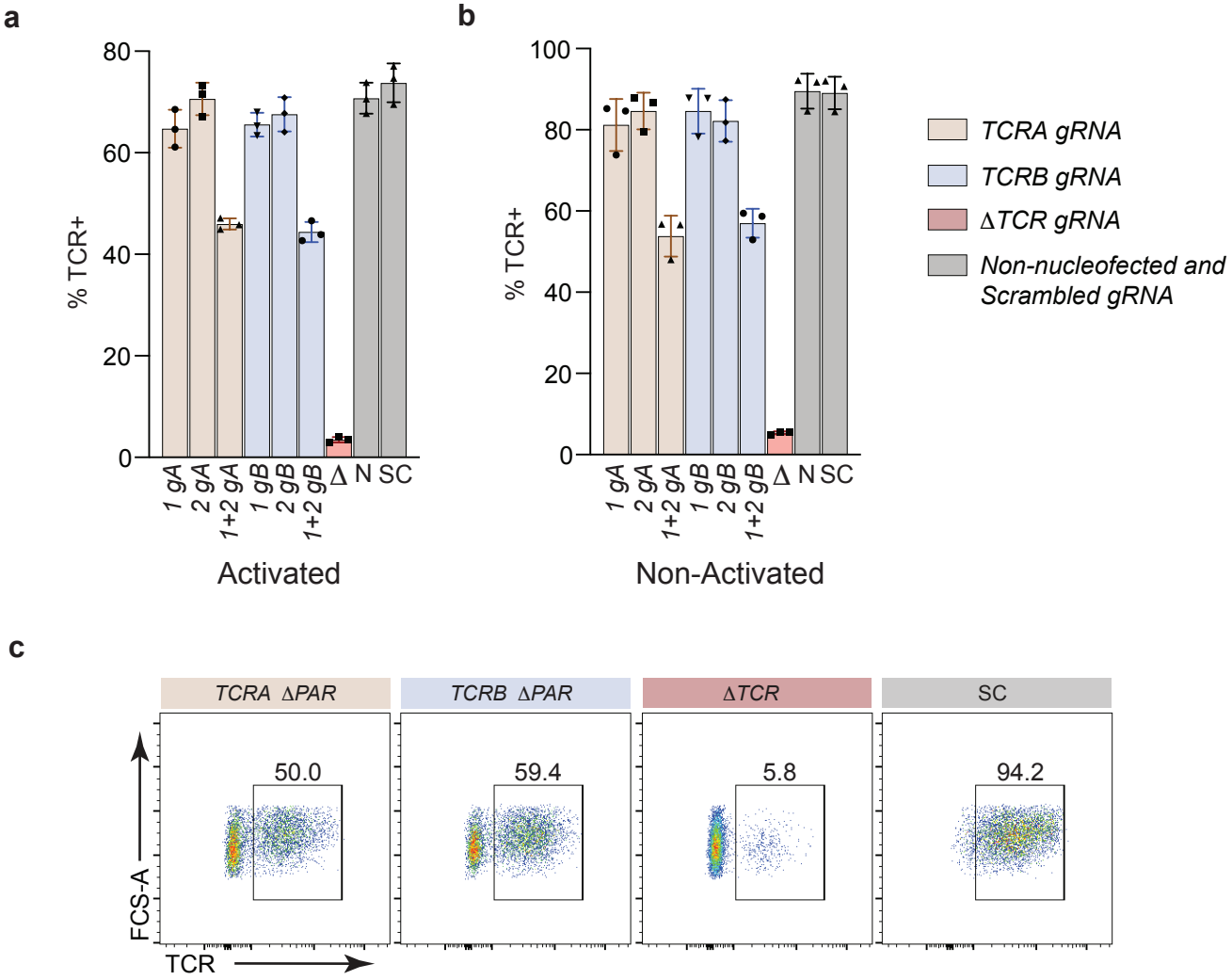

Extended Data Fig. 9

a

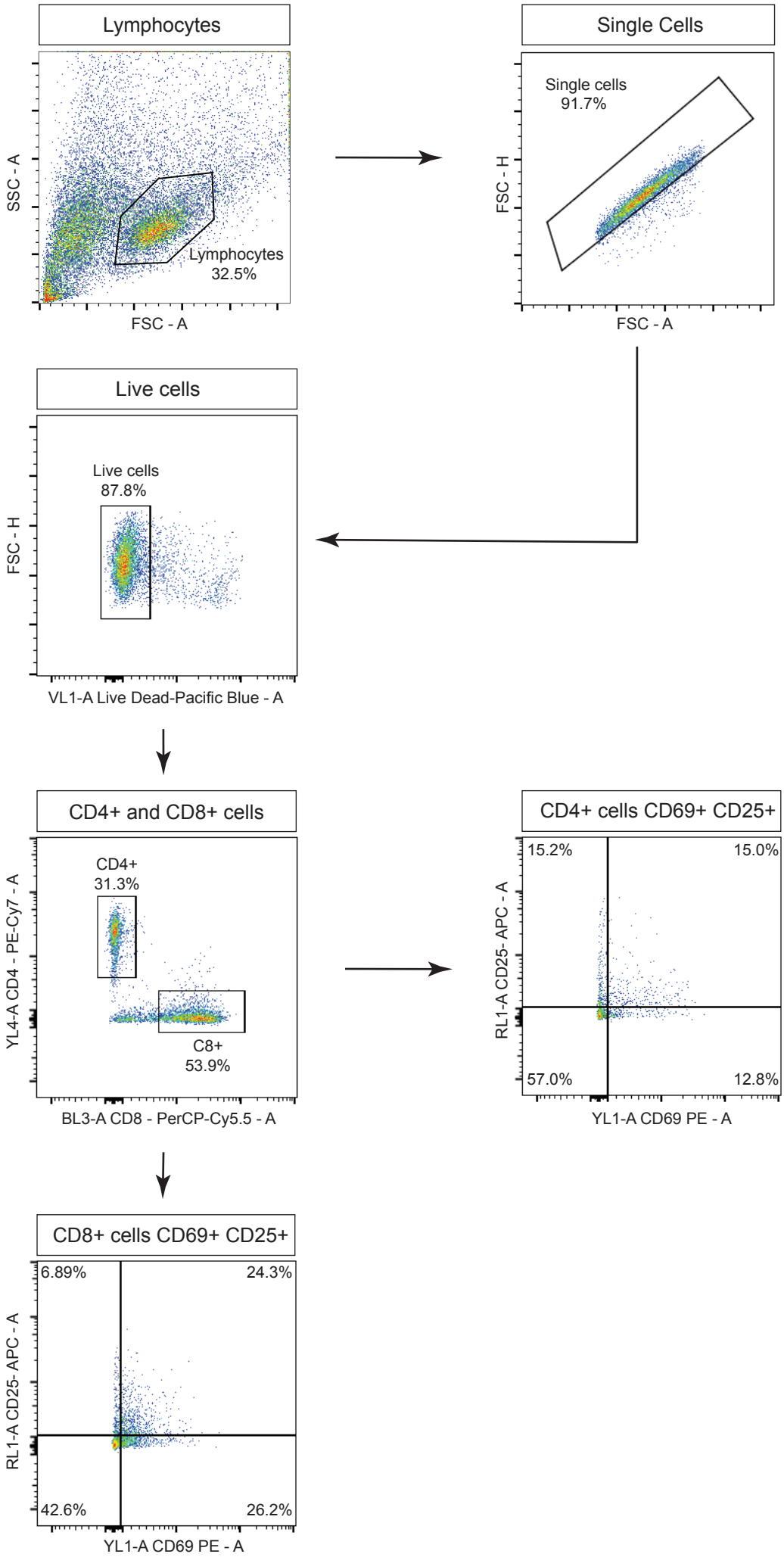

Extended Data Fig. 10

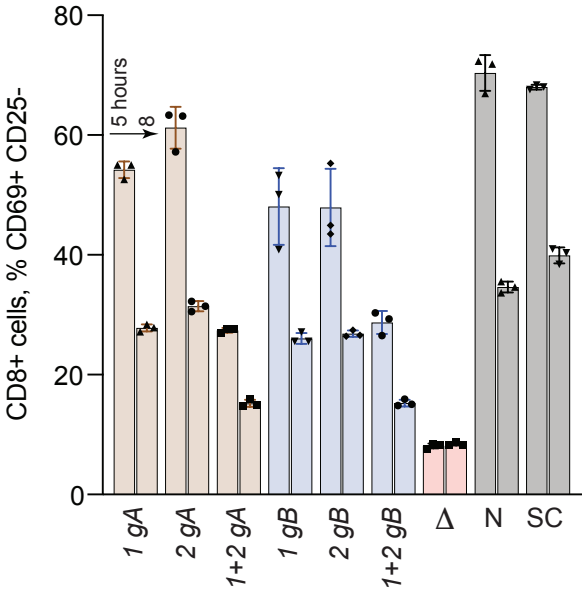

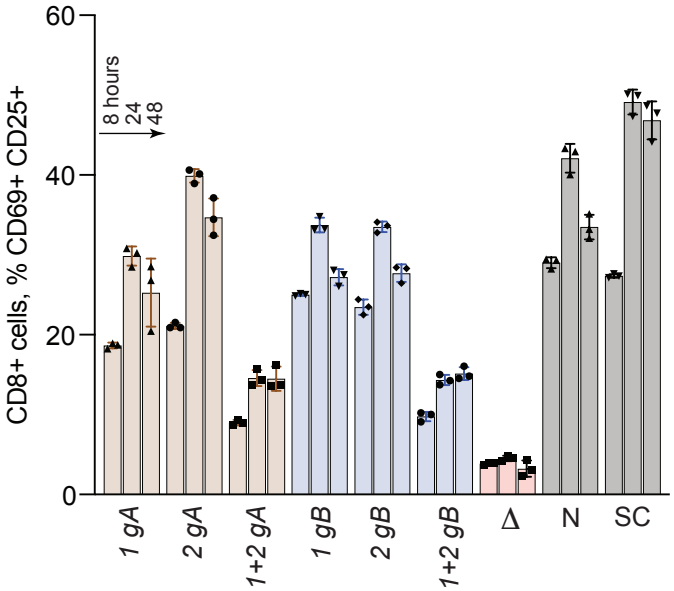

Extended Data Fig. 11

a

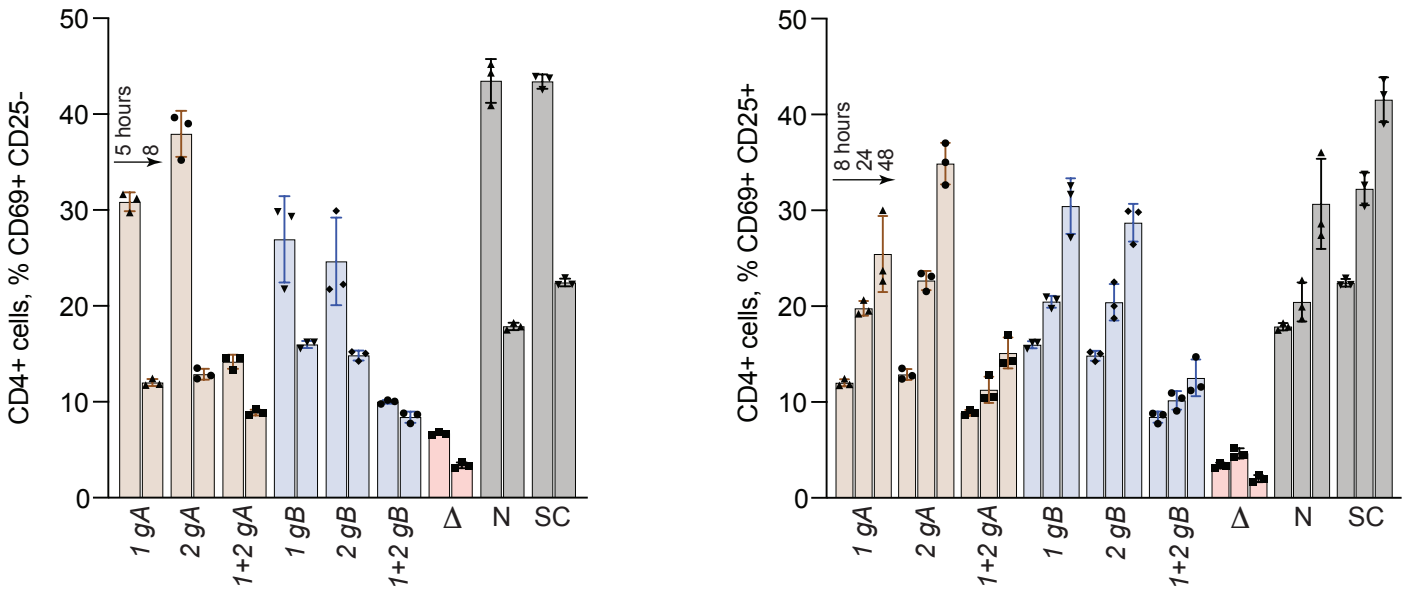

b

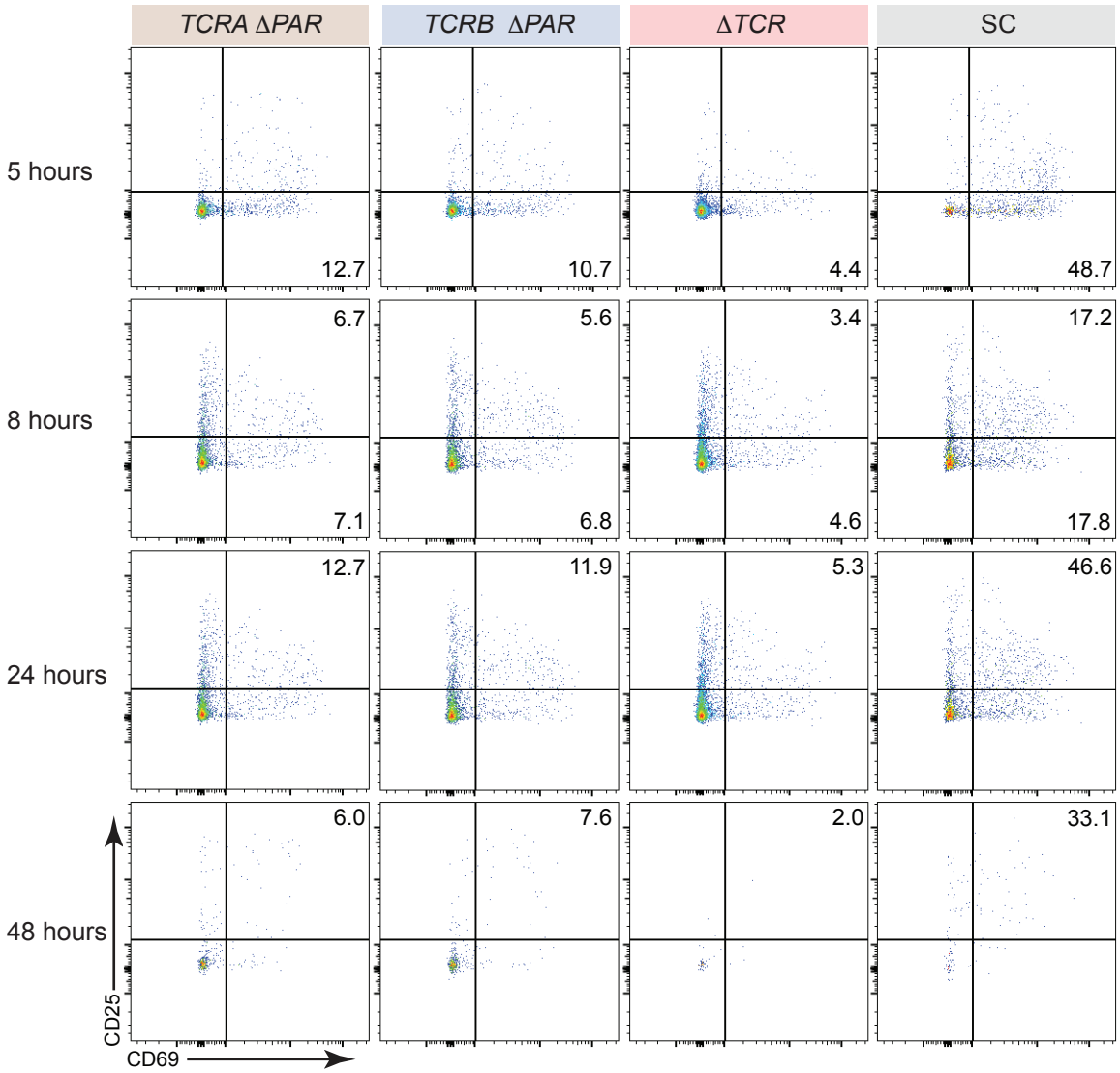

Extended Data Fig. 12

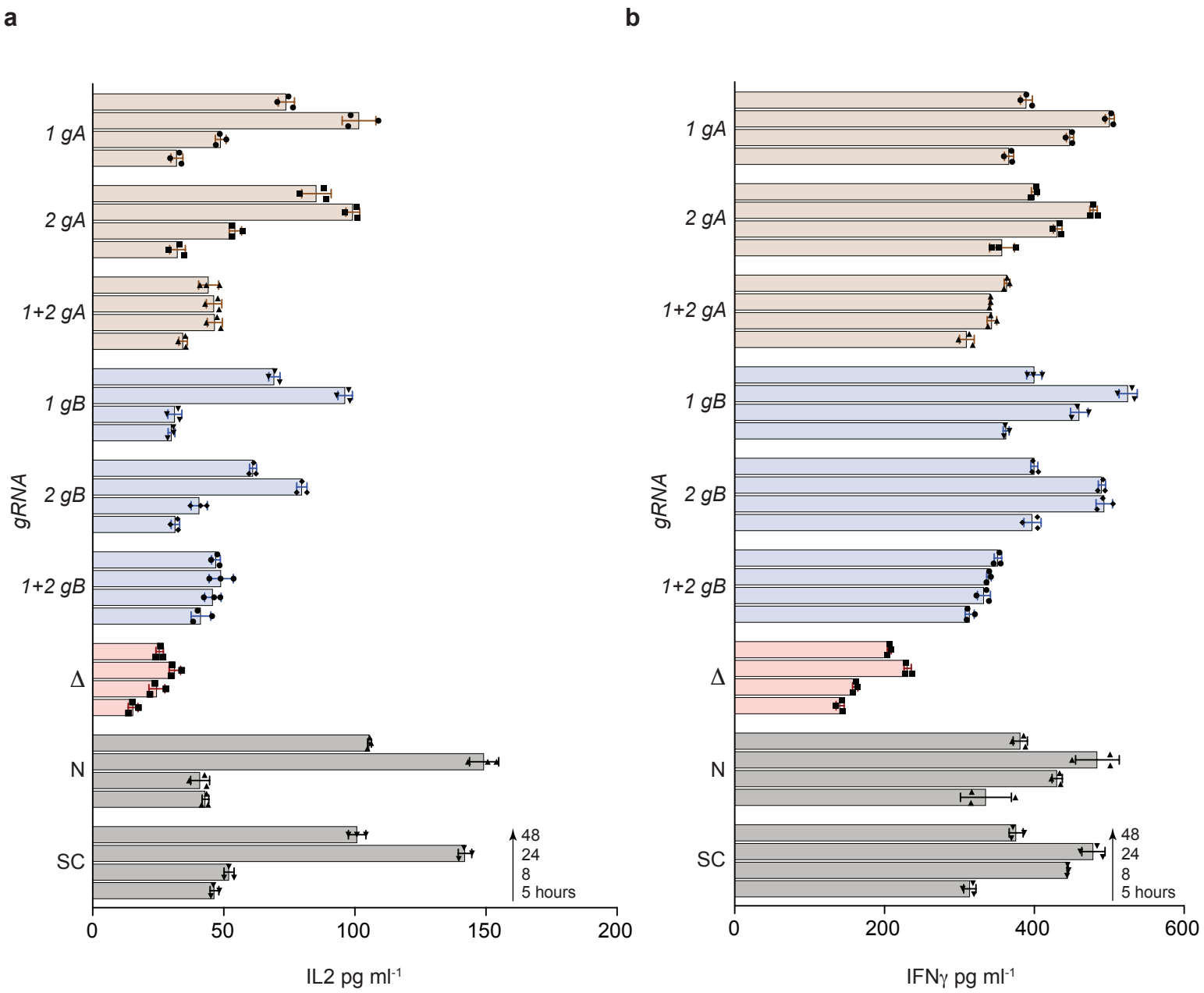

Extended Data Fig. 13

a

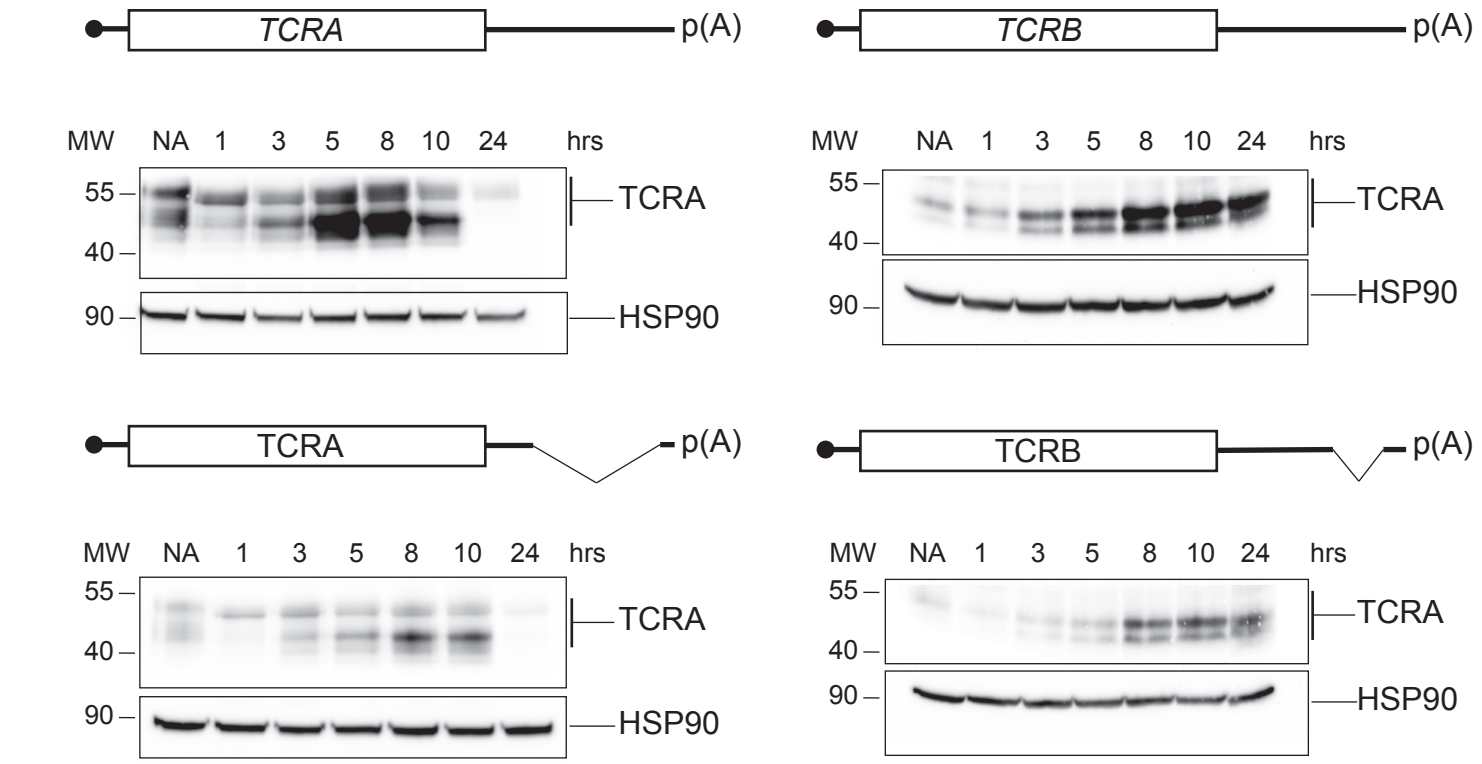

b

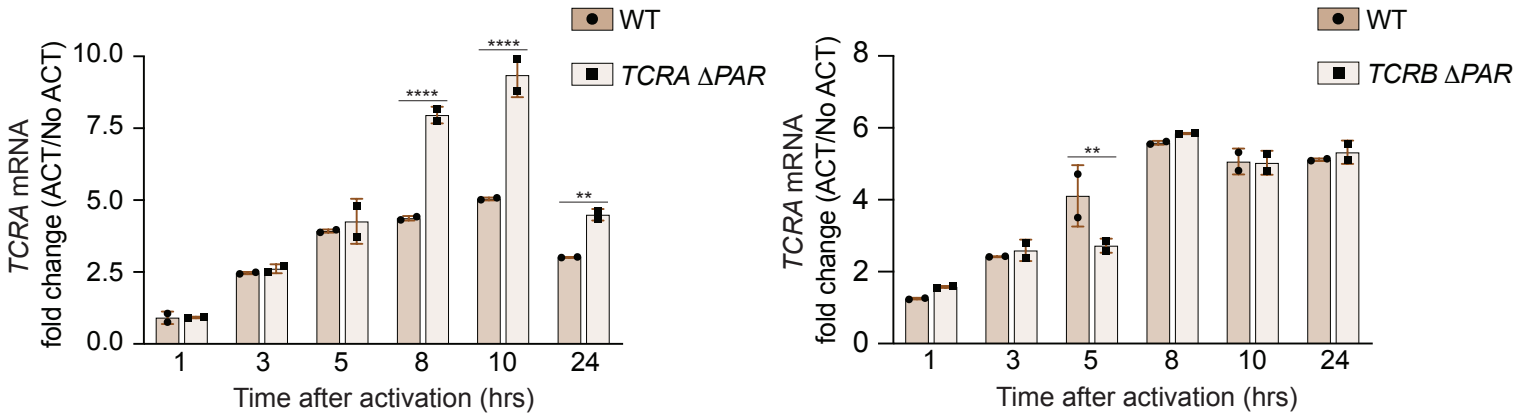

c

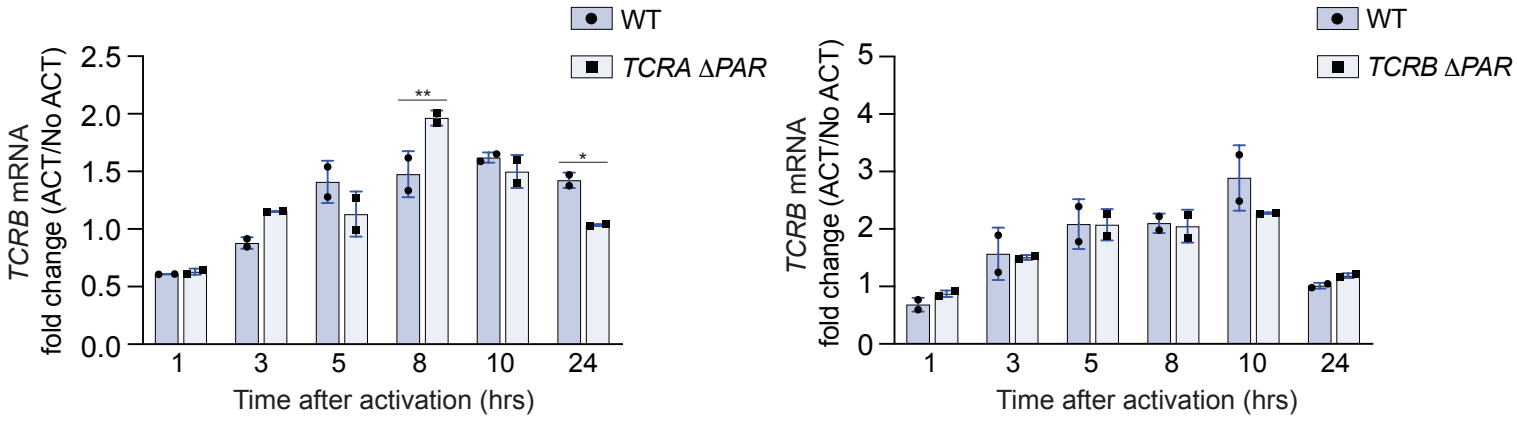

Extended Data Fig. 14

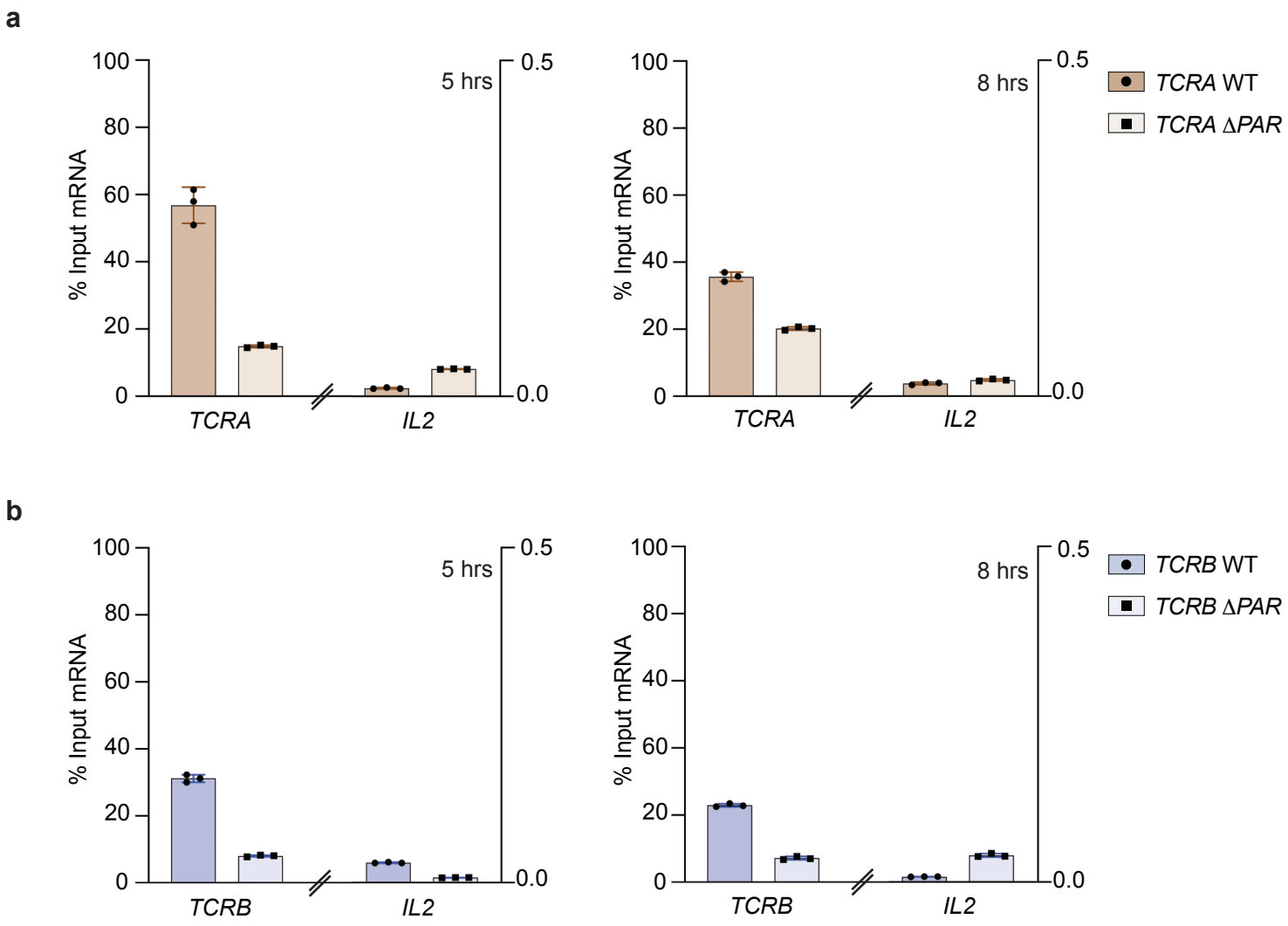

Extended Data Fig. 15

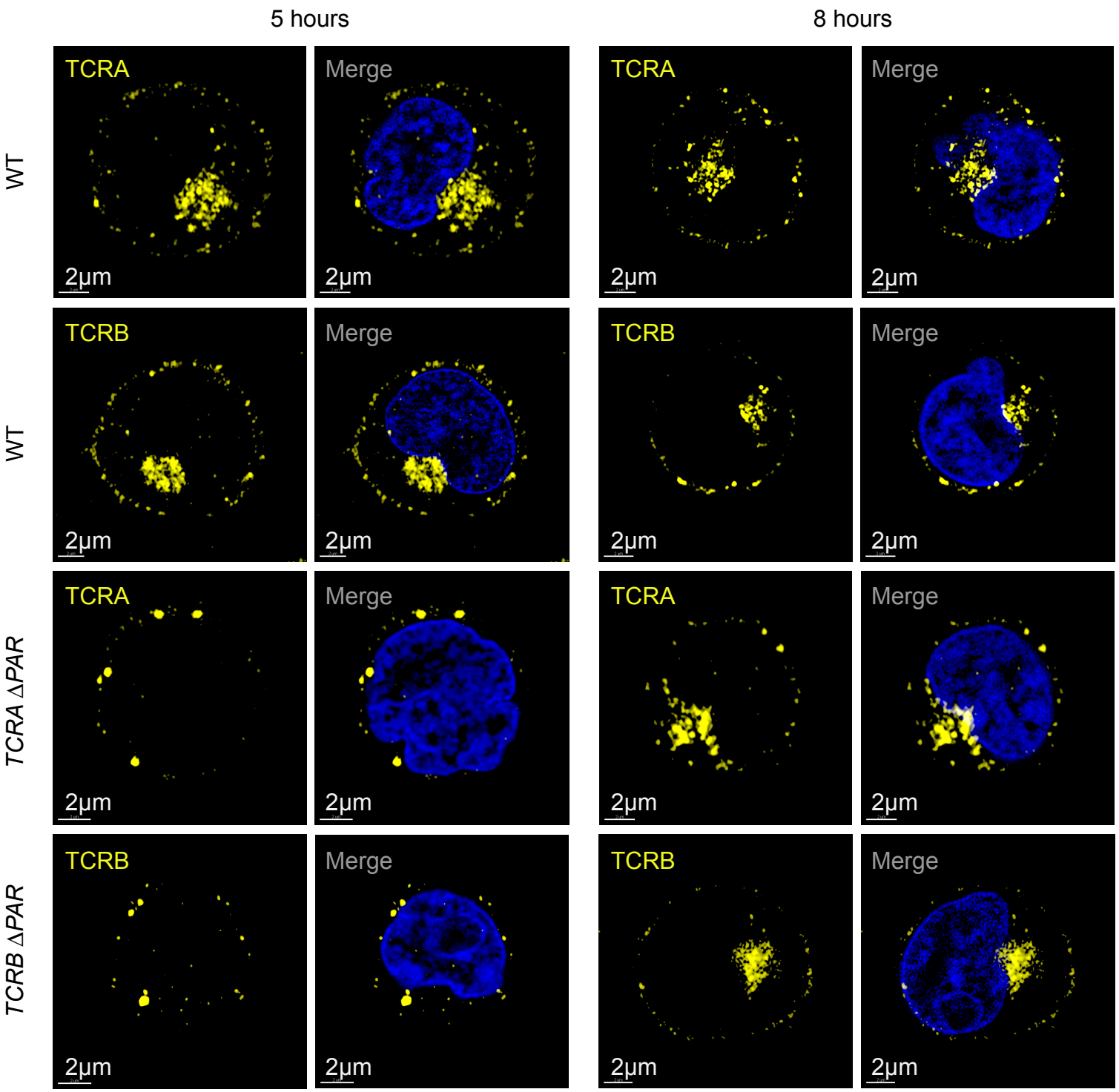
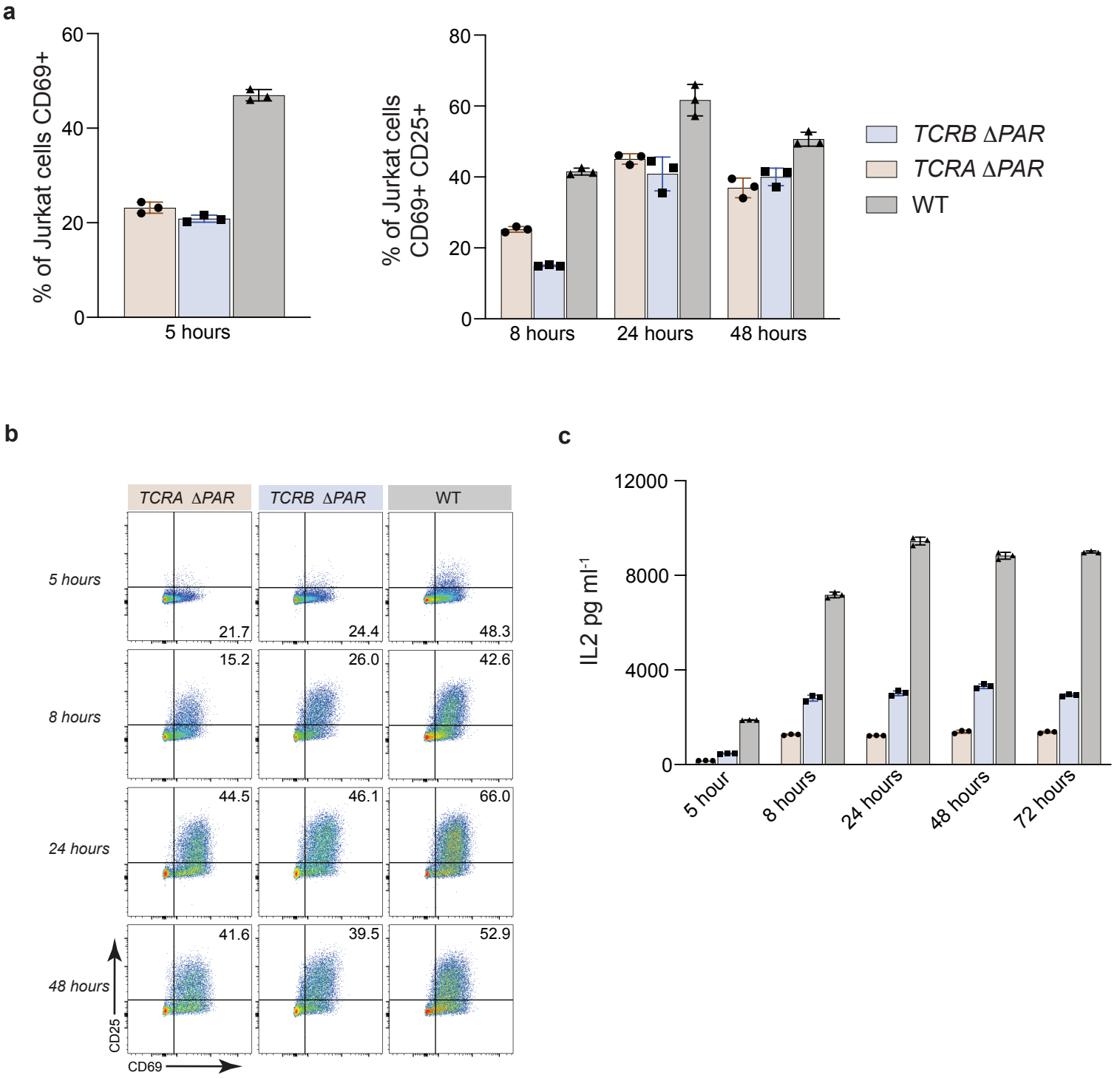
Extended Data Fig. 16